

Proton and antiproton cross sections at high energies

To cite this article: G Matthiae 1994 *Rep. Prog. Phys.* **57** 743

View the [article online](#) for updates and enhancements.

You may also like

- [Diffractive focusing of a uniform Bose–Einstein condensate](#)
Patrick Boegel, Matthias Meister, Jan-Niclas Siemß et al.
- [Axial focusing characteristics of diffractive micro-lenses based on a rigorous electromagnetic theory](#)
Di Feng, Yingbai Yan, Guofan Jin et al.
- [Microtechnology in computer optics](#)
V A Danilov

Proton and antiproton cross sections at high energies

G Matthiae

Dipartimento di Fisica, Università di Roma II, Tor Vergata, Italy
and INFN, Sezione di Roma Tor Vergata, Italy

Abstract

Measurements of the total cross section and of diffractive processes, which have been performed in the last decade at the high-energy hadron colliders, are presented and compared with earlier results at lower energy. The general properties of the scattering amplitude, as derived from fundamental principles, are discussed, together with the current models and with the recent theoretical developments based on QCD.

This review was received in February 1994

Contents

	Page
1. Introduction	745
2. Definitions	746
3. General properties of the amplitude	748
3.1. Bounds on the scattering amplitude	750
3.2. Particle and antiparticle reactions	752
4. Regge models	752
5. Diffraction models	755
5.1. The geometrical picture	755
5.2. The impact picture	756
5.3. The multiple-diffraction model	759
5.4. A model with fluctuations in the eikonal	760
6. QCD models	761
7. Experimental methods	762
7.1. Elastic scattering	763
7.2. Total cross section	764
7.3. The real part in the forward direction	765
8. Experimental results on σ_{tot} and $d\sigma/dt$	766
8.1. Total cross section and real part	766
8.2. The ratio of the elastic to the total cross section	770
8.3. The forward peak	771
8.4. The dip-shoulder region	774
8.5. The large-momentum-transfer region	779
9. Diffraction dissociation	782
9.1. General features	782
9.2. Differential distributions	784
9.3. The integrated cross section σ_{SD}	786
10. Conclusions and outlook	787
References	788

1. Introduction

The present review is mainly devoted to a general discussion of the total cross section and elastic scattering of strongly interacting particles at high energy. Moreover, the related subject of diffraction dissociation will also be treated in some detail.

Traditionally, the study of the total cross section, which measures the overall probability of interaction, has played a crucial role in nuclear and particle physics. At energies in the centre-of-mass system (CMS) below a few GeV, the total cross section of strongly interacting particles (hadrons) usually has a complex structure with peaks, or resonances, which reveal the formation of excited hadronic states. At higher energies a common feature of all hadron-nucleon cross sections is a smooth behaviour.

The first clear experimental evidence that the total cross sections grow with energy was reported in 1972 from measurements on proton-proton collisions at the CERN intersecting storage rings (ISR) in the CMS interval of energy from 20 GeV up to about 50 GeV. Later the measurements at Fermilab on pion-proton and kaon-proton collisions demonstrated that rising with energy is a common property of all hadron-nucleon total cross sections.

In the '80s the advent of the new proton-antiproton machines, the SPS collider at CERN and the Tevatron at Fermilab, opened a new energy domain (CMS energy from 0.5 TeV up to 1.8 TeV) giving some new insight on the mechanism of growth of the total cross sections. Recent cosmic ray data which extend up to CMS energies as large as 30 TeV have also provided relevant information on this subject.

In addition to the total cross sections, elastic scattering has been thoroughly investigated, especially for proton-proton and proton-antiproton interactions. Some of the elastic scattering data extend to large values of the momentum transfer, thus providing important insight on the dynamical mechanism of high-energy collisions. Similarity and differences between pp and $\bar{p}p$ scattering have been carefully studied.

The prominent feature which emerges from the data is that the effective range of interaction of the colliding hadrons increases with energy. Moreover, the absorption probability also increases. In a qualitative picture the particles appear to 'expand' and become more 'opaque' at high energy.

In this article, we first present in section 3 a short review of the general properties of the scattering amplitude which are derived from fundamental principles and are therefore model-independent.

A survey of the theoretical ideas which are incorporated into current models is made in sections 4 and 5. At present several models may rightly claim to be successful in the phenomenological description of high-energy scattering, but a real theory is still missing.

According to the common and well founded belief, quantum chromodynamics (QCD) is the underlying theory. QCD had a remarkable success in the description of large momentum-transfer processes where the constituents of the hadrons (quarks) behave to some extent as free particles. In this case the perturbative approach retains its validity. On the other hand, in the low-momentum-transfer domain of the so-called 'soft collisions' the effective coupling constant of strong interactions is large and the perturbative approach is no longer applicable. This explains why we do not at present have a theory for high-energy scattering but we observe a proliferation of 'QCD-inspired' models. Various attempts toward a QCD description of high-energy scattering, will be mentioned in section 6.

The measurements of elastic scattering and of the total cross section at the high-energy hadron colliders are not trivial. It was necessary to develop special techniques for this specific problem. The experimental methods and their limitations are discussed in section 7.

The review of the experimental results on total cross section and elastic scattering

(section 8) will essentially be concentrated on the data obtained in the last decade at the high-energy accelerators, i.e. the SPS collider and the Tevatron. Earlier results at lower energy will be mentioned only when relevant in connection with the more recent data.

The process of diffraction dissociation, a two-body inelastic reaction without exchange of quantum numbers, which may be considered as a kind of 'quasi-elastic' scattering will be discussed in section 9.

Several review papers on the subject of high-energy scattering have appeared in the last few years. We mention here the articles on the measurements at the SPS collider (Castaldi and Sanguinetti 1985, Martin and Matthiae 1989, Ward 1989), the recent review by Albrow (1993) which includes the last experimental results, and the critical discussion by Halzen (1993) on several aspects of present theoretical activity.

2. Definitions

In the discussion of the elastic-scattering reaction (Chew 1961) of particle a against particle b , it is useful to consider in addition to the main or direct process

$$a + b \rightarrow a + b \quad (1)$$

also the corresponding crossed processes in which one of the ingoing particles is replaced by an outgoing antiparticle, i.e.

$$a + \bar{a} \rightarrow b + \bar{b} \quad (2)$$

and

$$a + \bar{b} \rightarrow a + \bar{b}. \quad (3)$$

The kinematics is defined by the three invariant quantities s , t and u , also called Mandelstam variables, which are related by the equation

$$s + t + u = 2m_a^2 + 2m_b^2.$$

In the direct channel defined by (1), s represents the square of the CMS energy while t is the 4-momentum transfer squared which is written as

$$t = -2k^2(1 - \cos \theta)$$

where k is the CMS momentum and θ the scattering angle. The three processes related by crossing, as defined by (1)–(3), are also called s , t and u -channel, respectively.

In the formal theory of the scattering process one starts from the definition of the S -matrix and of the transition matrix T which transform the initial into the final state. Conservation of probability implies the unitarity of the S -matrix. The usual scattering amplitudes can be expressed in terms of the matrix elements of T in the momentum representation.

Assuming that spin effects can be ignored, we shall describe elastic scattering by a single invariant amplitude $F(s, t)$. The differential cross section $d\sigma/d\Omega$ (or $d\sigma/dt$) is given in terms of the amplitude F by

$$\frac{d\sigma}{dt} = \frac{\pi}{k^2} \frac{d\sigma}{d\Omega} = \frac{4\pi}{k^2 s} |F|^2. \quad (4)$$

A direct consequence of the unitarity of the S -matrix is the optical theorem which relates the imaginary part of the amplitude in the forward direction to the total cross section

$$\sigma_{\text{tot}} = \frac{8\pi}{k\sqrt{s}} \text{Im}F(t=0). \quad (5)$$

It is usual to introduce the parameter ρ , defined as the ratio of the real to the imaginary part of the forward amplitude,

$$\rho = \text{Re}F(t=0)/\text{Im}F(t=0). \quad (6)$$

At large energy, where $s \simeq 4k^2$, we may use the approximate relations

$$\frac{d\sigma}{dt} \simeq \frac{16\pi}{s^2} |F|^2 \quad \sigma_{\text{tot}} \simeq \frac{16\pi}{s} \text{Im}F(t=0).$$

The conventional amplitude $f(s, \cos\theta)$, defined by $d\sigma/d\Omega = |f|^2$ is related to the invariant amplitude F by

$$f = \frac{2}{\sqrt{s}} F \simeq F/k. \quad (7)$$

The usual expansion of the scattering amplitude in the partial-wave series is

$$F(s, \cos\theta) = \frac{\sqrt{s}}{2k} \sum (2l+1) f_l(s) P_l(\cos\theta) \quad (8)$$

where the partial-wave amplitudes $f_l(s)$ are given in terms of the phase shifts $\delta_l(s)$ by $f_l = (e^{2i\delta} - 1)/2i$. The optical theorem can then be written in terms of the partial waves as

$$\sigma_{\text{tot}} = \frac{4\pi}{k^2} \sum (2l+1) \text{Im}f_l. \quad (9)$$

Unitarity implies $|f_l|^2 \leq \text{Im}f_l \leq 1$.

We now introduce the impact parameter b , defined by $kb = l + \frac{1}{2}$. In a geometrical picture of the collision, the impact parameter has the semiclassical interpretation of minimum distance of approach between the two colliding particles. It becomes a very useful notion at high energy when the number of partial waves contributing to scattering is very large. Already at $\sqrt{s} = 20$ GeV, for a range of interaction of 1 fm, the number of partial waves which are involved in the scattering process is of the order of 100. It is therefore legitimate and often very convenient to rewrite the partial-wave expansion as an integral over the impact-parameter plane which is perpendicular to the incident momentum:

$$F(s, q) = \frac{is}{8\pi} \int e^{iq \cdot b} [1 - e^{-\Omega(s,b)}] d^2b \quad (10)$$

where $q^2 = -t$. This is sometimes called the eikonal approximation. The phase shifts are now replaced by the continuous function $\Omega(s, b)$, which is often called 'opacity' or 'eikonal'. The angular integration in (10) is readily performed and leads to express the amplitude as a Fourier-Bessel transform,

$$F(s, q) = \frac{is}{4} \int_0^\infty J_0(qb) [1 - e^{-\Omega(s,b)}] b db. \quad (11)$$

The 'profile' function $\Gamma(s, b) = 1 - e^{-\Omega(s,b)}$ is obtained by inverting (11):

$$\Gamma(s, b) = \frac{4}{is} \int_0^\infty J_0(qb) F(s, q) q dq. \quad (12)$$

The unitarity condition in impact-parameter space reads

$$G_{\text{in}}(s, b) = 2\text{Re}\Gamma(s, b) - |\Gamma(s, b)|^2$$

where $G_{\text{in}}(s, b)$ is the so-called 'inelastic' or 'shadow' profile function.

$$G_{\text{in}}(s, b) = 1 - |e^{-\Omega(s,b)}|^2. \quad (13)$$

It is the Fourier transform of Van Hove's (1964) inelastic overlap function and represents the probability of absorption which is associated with each value of the impact parameter b . By integrating the function $G_{\text{in}}(s, b)$ over the impact-parameter plane one gets the inelastic cross section

$$\sigma_{\text{in}}(s) = \int G_{\text{in}}(s, b) d^2b$$

while the total cross section is given by

$$\sigma_{\text{tot}} = 2 \int (1 - e^{-\Omega(s, b)}) d^2b.$$

3. General properties of the amplitude

Great effort has been spent to describe high-energy hadron scattering by using only a few general principles of relativistic quantum-field theory. An historical review of this field of theoretical activity is given in a recent paper by Martin (1993) which also contains reference to the most important contributions.

In the early '60s the motivation to pursue this theoretical approach was the lack of a dynamical theory of the strong interactions and also the belief that the description of scattering should become simpler as the energy increases. In fact, at high energy, with the number of partial waves which are involved very large, an accurate knowledge of each of them actually becomes irrelevant and a small number of parameters should be sufficient to describe high-energy collisions in a satisfactory way. These motivations remain essentially valid today because at present the low-momentum-transfer processes which contribute to most of the total cross section and the diffractive reactions cannot be treated perturbatively and calculated in a reliable way within QCD.

The fundamental principles which are used in this context are, in addition to Lorentz invariance, given by the following.

- (i) Analyticity which descends from the principle of causality. It states that the scattering amplitudes when expressed as a function of the appropriate kinematical variables can be continued analytically into the complex domain and the resulting analytic function has a simple singularity structure or at least the simplest one which is consistent with the other principles.
- (ii) Unitarity of the S -matrix which is a consequence of the principle of conservation of probability.
- (iii) Crossing symmetry which states that the invariant amplitudes describing elastic scattering in the s , t and u channels which *a priori* might be thought as independent, are actually embodied in a single analytic function $F(s, t, u)$.

Direct and very important consequences of analyticity are the dispersion relations which relate the real and the imaginary part of the scattering amplitude. In the simple and most useful form a dispersion relation allows us to write the real part at $t = 0$ as an energy integral involving the total cross section.

For the special case of proton-proton and proton-antiproton scattering, neglecting pole terms which are irrelevant at high energy, the once subtracted dispersion relations can be written as (Söding 1964)

$$\rho_{p, \bar{p}}(E) \sigma_{p, \bar{p}}(E) = \frac{A}{p} + \frac{E}{\pi p} \int_m^\infty dE' p' \left[\frac{\sigma_{p, \bar{p}}(E')}{E'(E' - E)} - \frac{\sigma_{\bar{p}, p}(E')}{E'(E' + E)} \right] \quad (14)$$

where E and p are the laboratory energy and momentum of the incoming particle and A is the subtraction constant. The parameter ρ is defined by (6). The subscripts p and \bar{p} refer to pp and to $\bar{p}p$ scattering respectively.

When discussing proton-proton and proton-antiproton collisions it is useful to introduce the even and odd signature amplitudes. The even signature amplitude is $F_+ = (F_{p\bar{p}} + F_{pp})/2$, while the odd signature amplitude is $F_- = (F_{p\bar{p}} - F_{pp})/2$. From these amplitudes one defines in the usual way σ_+ , σ_- and ρ_+ , ρ_- . If we assume that at high energy the odd-signature amplitude becomes negligible, then from (14) we get the following simple expression for the even signature amplitude:

$$\rho_+(E)\sigma_+(E) = \frac{2E}{\pi} \int_m^\infty dE' \frac{\sigma_+(E')}{E'^2(E' - E)^2}. \tag{15}$$

A simplified form of dispersion relations known as 'derivative dispersion relations' (Bronzan *et al* 1974) exhibits in a straightforward way the connection between the parameter ρ and the energy dependence of the total cross section. The derivative relations are valid when the energy dependence of the total cross section is sufficiently smooth as is the case at high energy. For the even signature amplitude one has

$$\rho_+ = \frac{1}{\sigma_+} \tan \left(\frac{\pi}{2} \frac{d\sigma_+}{d \log s} \right) \simeq \frac{\pi}{2\sigma_+} \frac{d\sigma_+}{d \log s}. \tag{16}$$

In the region where the total cross section is first decreasing with energy and then rising, we expect that ρ , which is initially negative, will rise, going through zero when the cross section has a minimum, becoming positive at high energy. This behaviour is indeed observed in all elastic hadronic reactions. If asymptotically $\sigma_{tot} \sim (\log s)^2$, then ρ will reach a broad maximum and then slowly decrease toward zero as $\pi/\log s$.

The connection between the real part and the total cross section was first established in a rigorous way by Khuri and Kinoshita (1965). The physical content of the theorems by Khuri and Kinoshita is presented in figure 1 where the behaviour of the parameter ρ is shown for different assumptions on the energy dependence of the total cross section.

This correlation between ρ and σ_{tot} has been exploited to make predictions on σ_{tot} at energies higher than those at which measurements were actually performed. Examples of these predictions made several years ago by Amaldi *et al* (1977) for $\bar{p}p$ and pp scattering and by Burq *et al* (1983) for π^+p and π^-p scattering are shown in figure 2.

Since then, higher energy data have become available only for $\bar{p}p$. The result obtained

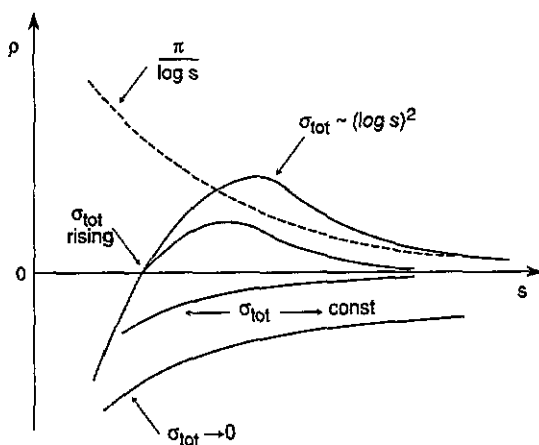


Figure 1. Behaviour of the parameter ρ (ratio of the real to the imaginary part of the forward amplitude) for different assumptions on the energy dependence of the total cross section. After Khuri and Kinoshita (1965).

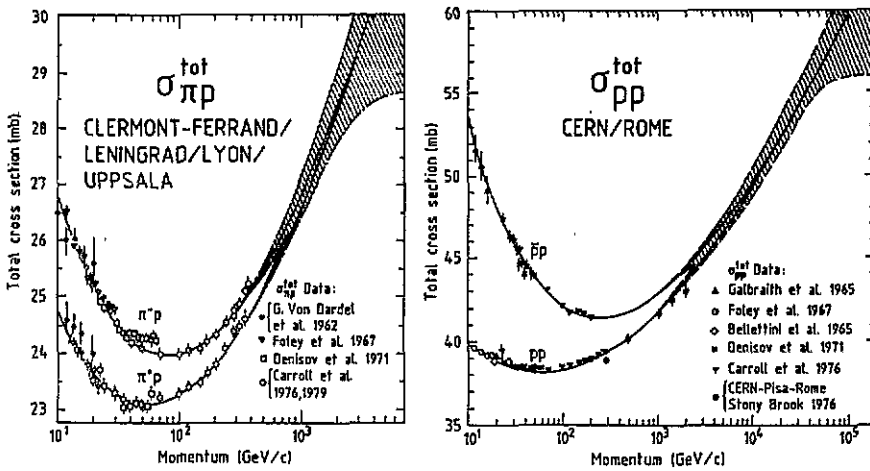


Figure 2. Predictions based on measurements of the real part of the high-energy behaviour of the total cross section from Amaldi *et al* (1977) and Burq *et al* (1983).

by the UA4 collaboration (Bozzo *et al* 1984c) at the CERN SPS collider ($\sqrt{s} = 546$ GeV) was $\sigma_{\text{tot}} = 62.2 \pm 1.5$ mb which is well within the range of the predicted extrapolation.

3.1. Bounds on the scattering amplitude

Several 'theorems' on high-energy collisions have been derived using the fundamental principles of analyticity, unitarity and crossing symmetry. These theorems are usually expressed in the form of mathematically rigorous inequalities which must be satisfied by the scattering amplitude. Here we only mention the most important results while for details and derivation we refer the reader to the specialized reviews on the subject (Roy 1972 and Fischer 1981).

A classical result on the high-energy behaviour of the total cross section is the famous Froissart–Martin bound, first derived by Froissart (1961) from the Mandelstam representation and then proved directly by Martin (1966) using analyticity and unitarity. This theorem states that asymptotically, i.e. as $s \rightarrow \infty$, the total cross section cannot increase faster than $(\log s)^2$; precisely,

$$\sigma_{\text{tot}} \leq \frac{\pi}{m_{\pi}^2} (\log s)^2. \quad (17)$$

The physical content of the Froissart–Martin bound can be expressed in the following way. At large energy the number of partial waves which effectively contribute to scattering is bounded by

$$L(s) \approx \frac{\sqrt{s} \log s}{4m_{\pi}}. \quad (18)$$

Unitarity puts the constraint $\text{Im} f_l \leq 1$ for $l \leq L(s)$. On the other hand for $l > L(s)$ the partial-wave amplitude is constrained by analyticity to be a fast decreasing function of l , with exponential bound,

$$\text{Im} f_l(s) \leq \exp\left(-\frac{4m_{\pi} l}{\sqrt{s}}\right).$$

This implies that asymptotically the contribution to the total cross section of the partial waves for $l > L(s)$ increases only as $\log s$. Asymptotically, the dominant contribution to σ_{tot} comes from the partial waves for $l \leq L(s)$. Using the unitarity constraint, from (9) and (18) one gets the bound given by (17).

After the discovery of the rise of the total cross sections there has been much discussion as to whether this rise might be related to the Froissart–Martin bound. As discussed in section 8.1, the data are consistent with a $(\log s)^2$ behaviour but the observed cross sections are numerically much smaller than the upper bound given by (17). In fact the numerical value of π/m_π^2 is about 60 mb. On the other hand it must be noted that the Froissart–Martin bound is a rigorous statement derived from general principles and therefore must be satisfied by any model of high-energy collisions for reasons of internal consistency.

On the integrated elastic cross section σ_{el} the following lower bound exists:

$$\sigma_{\text{el}} \geq \text{const} \frac{\sigma_{\text{tot}}^2(s)}{(\log s)^2}. \quad (19)$$

Bounds were also derived on the forward slope of the elastic differential cross section which is defined by

$$B(s, t = 0) = \frac{d}{dt} \left(\log \frac{d\sigma}{dt} \right)_{t=0}.$$

One of them corresponds to the Froissart–Martin bound on the total cross section

$$B(s, 0) \leq \text{const}(\log s)^2. \quad (20)$$

An important theorem is the lower bound known as the MacDowell–Martin (1964) relation, which is a consequence of unitarity and was derived exploiting the properties of the Legendre polynomials:

$$2 \left[\frac{d}{dt} \log \text{Im} F(s, t) \right]_{t=0} \geq \frac{1}{18\pi} \frac{\sigma_{\text{tot}}^2(s)}{\sigma_{\text{el}}(s)}. \quad (21)$$

If we neglect the real part of the amplitude at $t = 0$, then (21) gives

$$B(s, 0) \geq \frac{1}{18\pi} \frac{\sigma_{\text{tot}}^2(s)}{\sigma_{\text{el}}(s)}. \quad (22)$$

This bound was extended away from the forward direction but still in the low- t region by Singh and Roy (1970). We note the interesting fact that, contrary to most other asymptotic relations, the bound (22) appears to be almost saturated already at present energies. This is related to the fact that at high energy the shape of the differential cross section at low t can be approximately described by a simple exponential e^{Bt} , which implies $d\sigma/dt = B\sigma_{\text{el}} \exp(Bt)$. Then, for a purely imaginary amplitude, from the optical theorem one gets $B = (1/16\pi)\sigma_{\text{tot}}^2/\sigma_{\text{el}}$ which is very close to the bound (22).

Combining the previous bounds, one finds that if asymptotically the Froissart–Martin bound is saturated, i.e. if $\sigma_{\text{tot}}(s) \sim (\log s)^2$ then the elastic cross section and the forward slope will also follow the same behaviour and we expect $\sigma_{\text{el}}(s) \sim (\log s)^2$ and $B(s, 0) \sim (\log s)^2$. In that case the scattering amplitude acquires an important scaling property in the asymptotic regime (Auberson *et al* 1971). It becomes a function only of the variable $\tau = -t(\log s)^2 \sim -t\sigma_{\text{tot}}$,

$$F(s, t) = F(s, 0) \phi(\tau). \quad (23)$$

This formula was used as the basis for the ‘geometrical scaling’ model (Dias de Deus and Kroll 1978, Kroll 1983) which assumed that the asymptotic scaling law which holds if

the Froissart–Martin bound is saturated, is already valid at present energies. In this model the opacity function has the special scaling form, $\Omega(s, b) = \Omega[b/R(s)]$ with $R(s) \sim \log s$ and the ratio of the elastic to the total cross section is predicted to be a constant.

This model was quite successful in explaining some properties of elastic scattering at the ISR energies where the ratio σ_{el}/σ_{tot} indeed appears to be constant. However, later measurements at the SPS collider (Bozzo *et al* 1984c) have shown that σ_{el}/σ_{tot} increases with energy. As a consequence the notion of ‘geometrical scaling’ has only limited validity.

3.2. Particle and antiparticle reactions

Several theorems exist on the comparison between the cross sections for interaction of a particle and its own antiparticle on the same target. In the ‘60s when the total cross sections were assumed to reach a finite limit as $s \rightarrow \infty$, the comparison between particle–particle and particle–antiparticle cross sections was established by the Pomeranchuk theorem (1958) which stated that asymptotically

$$\sigma_{tot}(ab) = \sigma_{tot}(\bar{a}b). \quad (24)$$

Afterwards, when cross sections were found to increase with energy, the Pomeranchuk theorem was reformulated (Grunberg and Truong 1973) including the possibility of an indefinite rise as $(\log s)^2$. This ‘generalized’ Pomeranchuk theorem states that asymptotically

$$\frac{\sigma_{tot}(\bar{a}b)}{\sigma_{tot}(ab)} \rightarrow 1. \quad (25)$$

If the Froissart–Martin bound is saturated, it can be proven that

$$\sigma_{tot}(\bar{a}b) - \sigma_{tot}(ab) \leq C [\sigma_{tot}(\bar{a}b) + \sigma_{tot}(ab)] / (\log s). \quad (26)$$

This means that the total cross section difference between a particle and its antiparticle is allowed by general principles to increase with energy and even diverge asymptotically but it is bound by $(\log s)$.

A theorem similar to (25) exists for the ratio of the forward slopes of the differential cross section

$$\left[\frac{B(\bar{a}b)}{B(ab)} \right]_{t=0} \rightarrow 1. \quad (27)$$

As will be discussed in section 8, the experimental results on pp and $\bar{p}p$ from the ISR are consistent with these asymptotic predictions. Present data show that the total cross section difference $\Delta\sigma_{tot} = \sigma_{tot}(\bar{p}p) - \sigma_{tot}(pp)$ decreases with energy approximately as $s^{-1/2}$ for $\sqrt{s} \leq 60$ GeV. These results indicate that the odd signature amplitude F_- becomes negligible at high s and low t .

While this is the present common belief, or prejudice, as based on simple extrapolation of the trend of the available data, a different picture, the ‘odderon model’, was proposed (Lukaszuk and Nicolescu 1973, Kang and Nicolescu 1975, Gauron *et al* 1988). This unconventional model has the interesting feature that it satisfies all basic requirements of analyticity and unitarity and predicts $\Delta\sigma_{tot} \sim (\log s)$ asymptotically together with a saturation of the Froissart–Martin bound.

4. Regge models

The Regge theory has been successfully applied to describe two-body reactions at high energy and small momentum transfer. Comprehensive reviews (see for example Collins

1977) exist on the subject of Regge phenomenology. Here we only recall the basic concepts and the most useful formulae of the model.

The amplitude corresponding to the exchange of a single 'Regge pole' has the form

$$F(s, t) \sim \beta(t) \{1 \pm \exp[-i\pi\alpha(t)]\} s^{\alpha(t)} \quad (28)$$

where $\alpha(t)$ is known as the trajectory function while the quantity $\beta(t)$ is the residue function and the term in curly brackets is called the signature factor.

The exchange of a Regge pole in the t -channel actually corresponds to the exchange of an infinite series of particles (or resonances) with quantum number such that they may be formed in the crossed t -channel, $a + \bar{a} \rightarrow b + \bar{b}$. In fact at any given value of t , the contribution of a Regge pole with trajectory $\alpha(t)$ has the same s -dependence as the exchange of a particle whose spin is equal to $\alpha(t)$. Information on the trajectory function $\alpha(t)$ is inferred from the plot of the spin of known resonances versus the square of their mass. The trajectories appear to be approximately linear in t and therefore one may write $\alpha(t) \simeq \alpha(0) + \alpha' t$.

The contribution of a given Regge pole to the total cross section is determined by the value of the intercept $\alpha(0)$ of the trajectory at $t = 0$,

$$\sigma_{\text{tot}} \sim s^{\alpha(0)-1} \quad (29)$$

The differential cross section corresponding to the amplitude (28) can be written as

$$\frac{d\sigma}{dt} \sim H(t) s^{2\alpha(0)-2} e^{(2\alpha' \log s)t} \quad (30)$$

where $H(t)$ is a slowly varying function of t .

Equation (30) shows that Regge exchange with linear trajectory predicts an exponential fall-off of the t -distribution, i.e. a form e^{Bt} , with a slope parameter B which increases logarithmically with energy. In the '60s these simple predictions were found to be approximately verified in all hadron-hadron scattering processes thus making Regge theory very popular.

At that time the total cross sections were observed to flatten off or to be slowly decreasing with energy, so it was clear that the exchange of 'normal' Regge poles, while quite effective to explain inelastic two-body reactions, could not be sufficient to describe elastic scattering. In fact Regge trajectories corresponding to the known resonances, have intercept $\alpha(0)$ of about $\frac{1}{2}$ (or less) which implies the energy dependence $\sigma_{\text{tot}} \sim s^{-1/2}$.

This led to the introduction of a special Regge trajectory called 'Pomeron' with the quantum numbers of the vacuum and with intercept $\alpha(0) \simeq 1$. It was assumed that the exchange of the Pomeron would describe, in a compact phenomenological fashion, the very complicated effect of absorption, i.e. the shadow on elastic scattering of the many inelastic channels which are open in high-energy collisions. The discovery that all hadron-hadron total cross sections grow with energy implies, within the Regge picture, that the Pomeron trajectory has an intercept which is slightly above 1.

Regge theory is able to provide a rather good description of the total cross sections as shown by Donnachie and Landshoff (1992) who fitted available data on all hadron-proton reactions for $\sqrt{s} \geq 6$ GeV with the simple expression

$$\sigma_{\text{tot}} = X s^{\alpha_P(0)-1} + Y s^{\alpha_R(0)-1} \quad (31)$$

where the first term corresponds to Pomeron exchange and the second to normal Regge exchange. Because the Pomeron has the quantum numbers of the vacuum, its coupling to a particle and to its antiparticle are equal so that the value of the coefficient X is the same for $\sigma_{\text{tot}}(ab)$ and for $\sigma_{\text{tot}}(\bar{a}b)$. In this model a single effective trajectory with $\alpha_R(0) \simeq \frac{1}{2}$ was

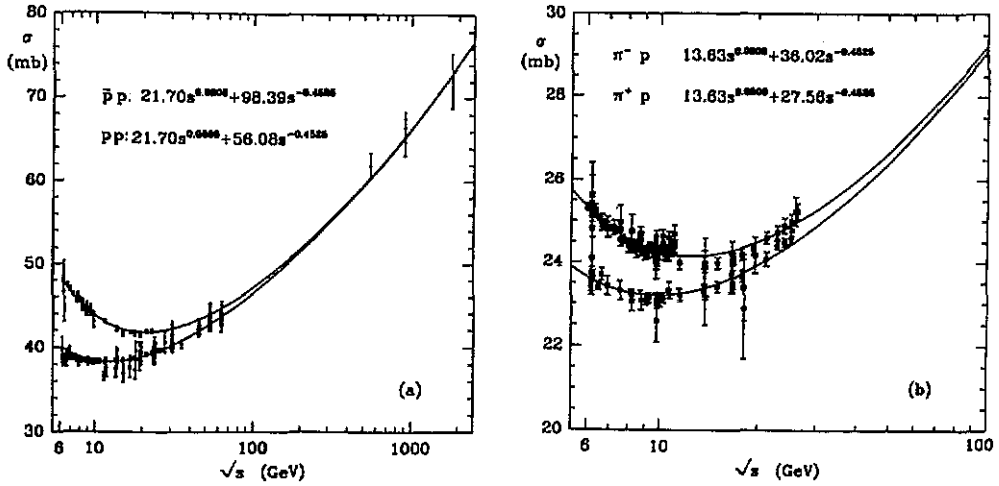


Figure 3. Regge model fit by Donnachie and Landshoff (1992) to the total cross sections of (a) $\bar{p}p$ and pp (b) $\pi^- p$ and $\pi^+ p$. Numerical values for the contributions of Pomeron and normal Regge exchange are also given.

used for normal Regge exchange while the intercept of the Pomeron was derived from an overall fit to the data. A good description of the total cross section data for $\bar{p}p$, pp , $\pi^\pm p$, $K^\pm p$ was obtained with $\alpha_P(0) = 1.0808$. The results for $\bar{p}p$, pp and $\pi^\pm p$ are shown in figure 3.

It is remarkable that reasonably good fits can be obtained with a small number of parameters. This study shows that the growth of the total cross sections occurs at the same rate for different channels and therefore is not connected to an intrinsic property of the hadrons but rather to the property of the exchanged system, the Pomeron.

It must be noted, however, that (31) with $\alpha(0) > 1$ is asymptotically not correct because it contradicts the Froissart–Martin bound and therefore violates unitarity. One may escape the contradiction by observing that this violation of the Froissart–Martin bound would only appear at enormous energies ($\sqrt{s} \sim 10^{27}$ GeV) and consider $\alpha_P(0)$ as an effective parameter with a slow energy dependence. Then the usual Regge picture would remain valid and useful in the present energy regime which is so far from ‘asymptotia’.

The Regge model becomes more sophisticated by reinterpreting the Regge amplitude of (28) as a kind of ‘Born approximation’. In that case higher-order terms corresponding to multiple Pomeron exchange will take care of restoring unitarity. An example of this approach is offered by the model of Covolan *et al* (1992 and 1993) where the Regge amplitude $F_{\text{Regge}}(s, t)$ is ‘eikonalized’ using the impact-parameter representation.

The procedure consists of expanding the exponential in (10), $e^{-\Omega} \simeq 1 - \Omega$, retaining only the first term which is linear in the eikonal Ω . One then obtains a first-approximation amplitude which is identified with the standard amplitude of the Regge theory,

$$F_{\text{Regge}}(s, q) = \frac{is}{4} \int_0^\infty J_0(qb)\Omega(s, b)b db. \tag{32}$$

The eikonal, which is obtained by inverting the previous equation,

$$\Omega(s, b) = \frac{4}{is} \int_0^\infty J_0(qb)F_{\text{Regge}}(s, q)q dq \tag{33}$$

is then inserted back into (10) in order to provide the full ‘eikonalized’ amplitude.

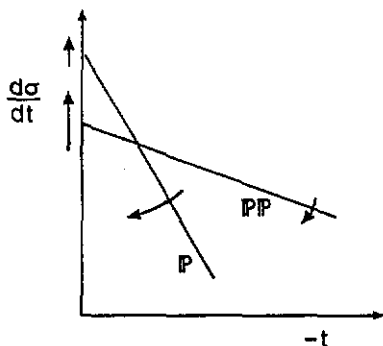


Figure 4. Contributions of single and double Pomeron exchange to the differential cross section of elastic scattering (Donnachie and Landshoff 1986). The arrows indicate how they change as the energy increases.

In this approach, terms corresponding to higher order Regge exchange have different energy and momentum-transfer dependence as shown in figure 4. The inclusion of these high-order amplitudes allows elastic scattering to be described not only near the forward direction where the differential cross section has a simple exponential shape, but also at larger values of the momentum transfer where a structure is observed.

5. Diffraction models

Hadron collisions at high energy exhibit the typical features of diffraction in the sense that at low momentum transfer the differential cross section of elastic scattering shows a sharp forward peak.

Diffraction theory applies when the wavelength of the wave being scattered is much smaller than the typical dimensions r_0 of the scattering system, i.e. when

$$kr_0 \gg 1.$$

With $r_0 \approx 1$ fm, this requirement is already satisfied at CMS energies of a few GeV. At these energies many inelastic channels are open and the absorption cross section is an important fraction (of the order of 80%) of the total cross section. Elastic scattering appears to be essentially the 'shadow' of the inelastic processes and the diffracted waves will add up coherently in the forward direction giving rise to a sharp forward peak.

Various diffraction models have been constructed with specific assumptions on the phase shift δ_1 or, equivalently, on the impact-parameter dependence of the opacity function Ω . Without additional input, however, these models cannot describe the energy dependence of the scattering process.

5.1. The geometrical picture

Historically, the first model which incorporated the basic ideas of diffraction theory was the geometrical picture proposed by Yang and collaborators (Chou and Yang 1968).

Starting from the remark that high-energy scattering is essentially the shadow of absorption, the two colliding hadrons are described as extended objects of some kind of 'hadronic matter' which fly through each other. At each space point the interaction probability will be proportional to the local density of hadronic matter which is assumed to have the same shape as the distribution of electric charge which is measured in electron-scattering experiments.

These ideas are naturally expressed in the impact-parameter formulation. The opacity (or eikonal) function $\Omega(s, b)$ defined in section 2 is assumed to be real, which implies a

purely imaginary scattering amplitude, and is written in the factorized form

$$\Omega(s, b) = K(s) T(b).$$

The function $T(b)$ describes the space distribution of the overlap of the two colliding particles projected on the impact-parameter plane. It is obtained from the Fourier–Bessel transform of the square of the electromagnetic form factor $G(q^2)$:

$$T(b) = \int_0^\infty J_0(qb) G^2(q^2) q dq.$$

The energy-dependent parameter $K(s)$ which measures the strength of the interaction is the only free parameter of the model. Its numerical value is adjusted to reproduce the measured total cross section.

The geometrical picture (Chou and Yang 1968, Durand and Lipes 1968) predicted that the differential cross section of elastic scattering would show a kind of diffraction pattern with sharp minima. Afterwards a dip was in fact observed in proton–proton scattering at the ISR for $-t \sim 1 \text{ GeV}^2$. Experimentally the dip is much less sharp than predicted by the model, which is expected, however, because in the model the real part of the amplitude is neglected.

Some simple scaling rules hold as direct consequences of the basic assumptions of the model: the momentum transfer of the dip is expected to vary as $1/\sigma_{\text{tot}}$ while the forward-slope parameter B should increase proportionally to σ_{tot} . These rules are in fact approximately verified experimentally.

The geometrical picture cannot predict the energy dependence of the parameter K . It predicted, however, a link between the total cross section, the ratio $\sigma_{\text{el}}/\sigma_{\text{tot}}$, and the value of $d\sigma/dt$ at the second maximum, just beyond the diffraction minimum (Chou and Yang 1979). As shown in figure 5, these predictions are qualitatively in agreement with later observations at the SPS collider and at the Tevatron.

In the asymptotic limit (Chou *et al* 1982), if $\sigma_{\text{tot}} \rightarrow \infty$, then $\sigma_{\text{el}}/\sigma_{\text{tot}}$ would approach $\frac{1}{2}$ and the amplitude would take the form

$$F(s, q) = i \frac{s R^2}{4} \frac{J_1(Rq)}{Rq} \quad (34)$$

which is just the familiar Fraunhofer formula for diffraction by a completely absorbing disk in optics.

The geometrical picture is a simple model and does not claim to be able to fit the data quantitatively. It was able, however, to evidenciate fundamental features of high-energy scattering and was seminal for further developments. The underlying physical concepts of the geometrical picture are shared by more elaborate diffraction models.

5.2. The impact picture

The impact picture is based on the original work of Cheng and Wu (1969) on quantum electrodynamics (QED), performed when QCD had not yet been developed. They assumed that some understanding of high-energy hadronic collisions could be obtained from the study of the asymptotic behaviour of high-order Feynman graphs in QED. The motivation was that relativistic quantum-field theory (which incorporates relativity and absorption, i.e. particle production) should be able to provide the basic clues for the right description of high-energy scattering, independently of the specific interaction, whether it is the electromagnetic interaction of electrons or the strong interaction of hadrons. The study of a special class of

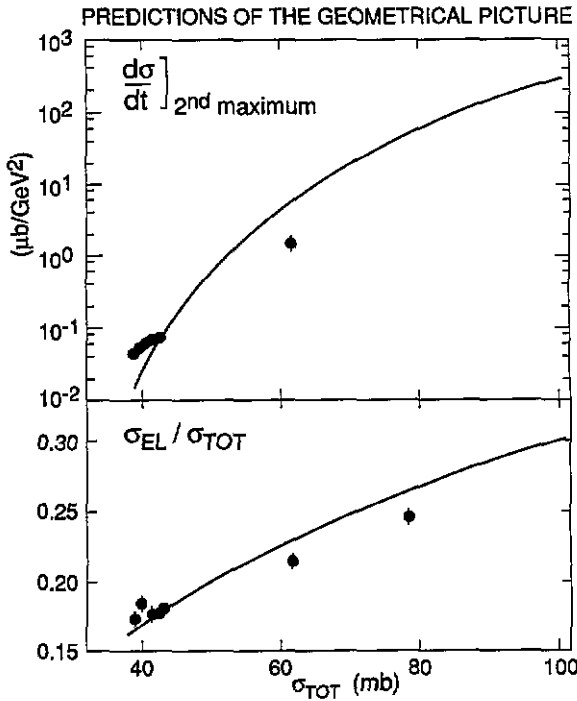


Figure 5. The predictions of the geometrical picture by Chou and Yang (1979), represented by the full lines, are compared to the experimental data.

'tower graphs' led Cheng and Wu (1970) to predict that the hadronic cross sections would grow with energy and asymptotically would saturate the Froissart–Martin bound.

More recently Bourrely *et al* (1984 and 1988), inspired by these results on QED, have developed a phenomenological model which has been quite successful in describing high-energy pp and $\bar{p}p$ scattering.

Their model is formulated in the impact-parameter formalism. The opacity function is written as

$$\Omega(s, b) = S(s) T(b) + R(s, b) \tag{35}$$

where the first term represents the diffraction component which is relevant at high energy while the second term is a Regge contribution that decreases quickly with energy. The first term is assumed to factorize to the product of a function of energy times a function of the impact parameter. The energy-dependent term is taken from the study of Cheng and Wu (1970) on QED. It is written in the crossing-symmetric form

$$S(s) = \frac{s^c}{(\log s)^{c'}} + \frac{u^c}{(\log u)^{c'}} \tag{36}$$

where u is the Mandelstam variable introduced in section 2 and c and c' are constant.

The function $T(b)$ which describes, as in the geometrical picture, the density distribution of the two overlapping hadrons, is derived from the charge density. With only four free parameters the model is able to correctly reproduce the experimental results on σ_{tot} , ρ and on the differential cross section of elastic scattering (Bourrely *et al* 1990).

The distinctive feature of the impact picture, when compared with other diffraction models, is the explicit use of an energy dependence which is obtained from quantum-field theory. The power term s^c in the opacity function leads asymptotically to the saturation of the Froissart–Martin bound.

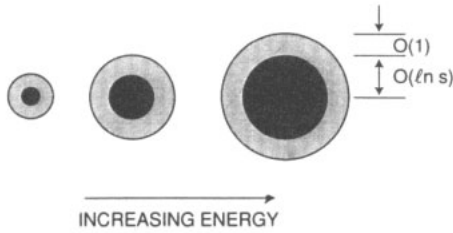


Figure 6. Graphical illustration of the 'expanding protons' in the impact picture of Cheng and Wu (1987).

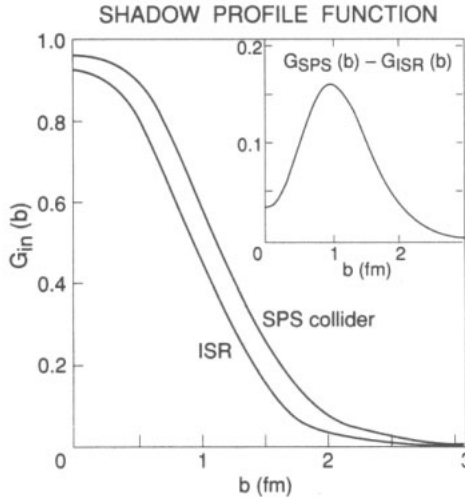


Figure 7. The shadow profile function G_{in} at $\sqrt{s} = 53$ GeV (ISR) and $\sqrt{s} = 546$ GeV (SPS collider) as derived from the data by Henzi and Valin (1983). The inset shows the change of G_{in} .

The model predicts that asymptotically σ_{tot} , σ_{el} and the slope B will all increase as $R(s)^2$ where $R(s)$ is a typical interaction radius which grows logarithmically with energy, $R(s) \simeq R_0 \log s$. The ratio σ_{el}/σ_{tot} is predicted to approach $\frac{1}{2}$ asymptotically.

The prediction that the total cross section would grow with energy together with the ratio of the elastic to the total cross section is a remarkable achievement of this model which has generally been demonstrated to possess a considerable predictive power (Cheng and Wu 1987).

The picture that emerges in this model is illustrated in figure 6. At high energy the two colliding hadrons have a 'central core', almost completely absorbing, with a radius growing as $\log s$, and a peripheral region, a 'gray fringe', only partially absorbing, whose width is energy-independent.

This prediction can be compared with the data by examining the energy variation of the shadow profile function $G_{in}(b)$. We note that the function $G_{in}(b)$ can be extracted directly from the t -dependence of the measured differential cross section of elastic scattering if that is known in a sufficiently wide interval of t . The procedure requires some assumption on the real part of the amplitude but it is almost model-independent (Amaldi and Schubert 1980).

Results on the shadow function at the ISR energy, $\sqrt{s} = 53$ GeV, and at the SPS collider energy, $\sqrt{s} = 546$ GeV, as derived from the data by Henzi and Valin (1983 and 1985) are presented in figure 7. The observed change from the ISR to the SPS is consistent with the predictions of the impact picture. Both the interaction radius and the central 'opacity' increase with energy. It is clear, however, that even at the large energy of the present accelerators, the central, 'opaque' region does not extend more than the 'gray edge'. This may give an idea of how far present energies are from the so-called 'asymptotic regime'

discussed in the theory.

5.3. The multiple-diffraction model

The multiple-diffraction theory was developed several years ago by Glauber (1959) to describe elastic scattering of hadrons by nuclei at high energy. The two basic ingredients of the theory are the amplitude of hadron–nucleon scattering and the nuclear-density distribution. Once these quantities are given, the amplitude for nuclear scattering can be calculated. It turns out that the nuclear amplitude can be expanded in a series in which the first term corresponds to single scattering of the incoming hadron by one nucleon of the target nucleus while the second term describes the sequence of two successive scattering processes by two nucleons and so on.

In view of the success obtained in describing nuclear collisions (Glauber 1969) the multiple-diffraction theory was recently extended by Glauber and Velasco (1984 and 1988) to high-energy hadron–hadron scattering. In this picture the two colliding hadrons are viewed as two clusters of interacting partons and the calculation of the hadron–hadron amplitude proceeds essentially in the same way as for nucleus–nucleus collisions.

For elastic scattering of hadron a against hadron b , the opacity function is written as

$$\Omega(s, b) = N_a N_b \int e^{-iq \cdot b} G_a(t) G_b(t) f_{\text{part}}(s, t) d^2q \quad (37)$$

where $q^2 = -t$. N_a and N_b are the number of partons present in the two hadrons. The elementary interaction between the hadronic constituents is described by the parton–parton scattering amplitude $f_{\text{part}}(s, t)$. The spatial distribution of partons in the hadrons a and b is assumed, as in the geometrical model, to be the same as the electric charge distribution. As a consequence the electromagnetic form factors $G_a(t)$ and $G_b(t)$ appear in (37).

The hadron–hadron scattering amplitude $F(s, t)$ is obtained by inserting the opacity (37) into the general form (10) of the amplitude. By expanding the exponential $e^{-\Omega(s, b)}$ in (10) in powers of Ω , the series expansion of the multiple-diffraction model can be written down explicitly. Retaining only the first term one gets

$$F(s, t) = G_a(t) G_b(t) f_{\text{part}}(s, t) \quad (38)$$

which represents the contribution of single parton–parton scattering. Higher-order terms of the series correspond to multiple parton–parton scattering processes.

It can be shown that the geometrical picture of Chou and Yang (section 5.1) corresponds to a particular case of the multiple-diffraction model, when the elementary parton–parton amplitude is taken to be isotropic.

Other models which make use of an approach very similar to the multiple-diffraction theory have been discussed by Menon (1992) and by Pumplin (1992). With a reasonably small number of free parameters all these models are able to reproduce the general features of elastic scattering at high energy.

The shape of the shadow profile function $G_{\text{in}}(b)$ as extracted from elastic scattering data at different energies by Glauber and Velasco (1988) is shown in figure 8. Previous results (section 5.2 and figure 7) on the increase of the central ‘opacity’ and of the effective-interaction radius with energy are confirmed by the multiple-diffraction analysis. In addition, this study reveals that in the peripheral region the shadow function has a dependence on the impact parameter which is very close to an exponential.

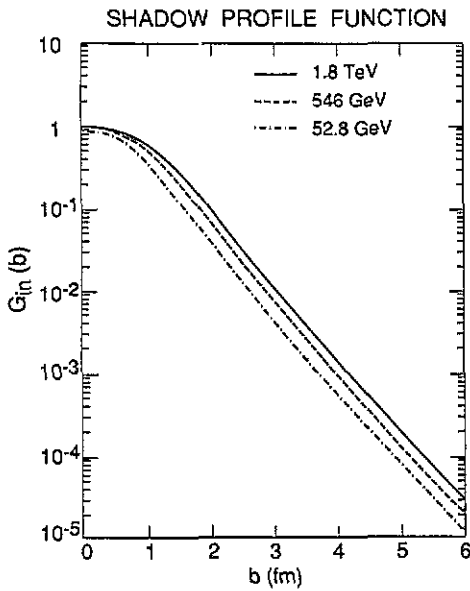


Figure 8. The shadow profile function G_{in} obtained in the multiple-diffraction model at different energies by Glauber and Velasco (1988).

5.4. A model with fluctuations in the eikonal

Several years ago it was recognized (Barshay 1972) that there is a connection between the opacity, or eikonal, function $\Omega(s, b)$ and the number distribution of particles produced in a collision, $n(s)$, which is a function of energy and fluctuates about the average $\langle n(s) \rangle$.

In an intuitive manner, central collisions occurring at low values of the impact parameter b are associated with large multiplicities while peripheral collisions which occur at large b lead to low-multiplicity events. Within this intuitive framework, the well known KNO scaling of the multiplicity distributions, first noticed by Koba *et al* (1972), was related (Dias de Deus 1973) to the notion of 'geometrical scaling' (section 3.1).

Afterwards, at the SPS collider energy, violations of both the geometrical scaling (increase of σ_{el}/σ_{tot}) and of the KNO scaling (Ward 1989) were observed. These two experimental facts were again considered as correlated.

In this context one is naturally led to the notion of a 'distribution' for the eikonal in the sense that specifying s and b fixes an average value $\langle \Omega(s, b) \rangle$ but significant fluctuations are expected about this average value (Barshay and Goldberg 1987). The probability distribution of the eikonal is assumed to have the same form which describes the multiplicity distribution of produced particles

$$P(\Omega, \langle \Omega \rangle) = \frac{k^k}{\Gamma(k)} \frac{1}{\langle \Omega \rangle} u^{k-1} e^{-ku}$$

where $u = \Omega/\langle \Omega \rangle$ and k is a parameter slowly decreasing with energy. The factor $(1 - e^{-\Omega})$ which appears in the expression of the scattering amplitude (11) is now replaced by

$$\int_0^\infty d\Omega P(\Omega, \langle \Omega \rangle) (1 - e^{-\Omega}) = \left(1 - \frac{1}{[1 + \langle \Omega(s, b) \rangle / k]^k} \right).$$

Once the impact-parameter dependence of the eikonal is fixed by the electromagnetic form factor, the model becomes specific and able to reproduce the data on high-energy scattering (Barshay *et al* 1992).

6. QCD models

The review article of Levin and Ryskin (1990) contains a rather general discussion of the attempts to formulate a theory of low-momentum-transfer processes based on perturbative QCD. Here we mention only a few important and representative developments in this field.

Various models of high-energy scattering fall in the class of the so-called 'QCD-inspired' models (Halzen 1993). They often lack mathematical rigour but have the merit of reformulating old concepts in a modern language with the aim of preparing a bridge toward a future theoretical description based on QCD.

A typical 'QCD-inspired' model was proposed by L'Heureux *et al* (1985) and developed by Margolis *et al* (1988) and Block *et al* (1990). In this model each of the two colliding protons is regarded as a collection of partons (quarks and gluons) each carrying a fraction x of the proton momentum. The transverse size of the proton is described by a profile function $T(b)$ derived from the proton form factor, as in the diffraction models. The opacity function is written as the sum of two terms

$$\Omega(s, b) = \Omega_{\text{vq}}(s, b) + \Omega_{\text{gg}}(s, b)$$

where Ω_{vq} accounts for the interaction of the valence quarks and Ω_{gg} describes the gluon-gluon interactions. The gluon term is responsible for the rise of the total cross section. It is written in the following form:

$$\Omega_{\text{gg}}(s, b) \sim T_{\text{gg}}(b) \int_0^1 dx_1 \int_0^1 dx_2 g(x_1)g(x_2)\sigma_{\text{gg}}(\hat{s})$$

which describes the interaction probability of a gluon with momentum fraction x_1 in the first proton colliding with a gluon with momentum fraction x_2 in the second proton. The quantity $\sqrt{\hat{s}}$ is the collision energy in the gluon-gluon system and is given by $\hat{s} = x_1 x_2 s$. The gluon-gluon cross section σ_{gg} is assumed to be constant above a certain threshold value which is of the order of 1 GeV. The distribution function of the gluons inside the proton, $g(x)$, is written in the usual form as

$$g(x) = N_g \frac{(1-x)^5}{x^J}.$$

The number of gluons present at low x , i.e. the number of gluons carrying a small fraction of the proton momentum, is determined by the parameter J which also controls the energy dependence of the opacity,

$$\Omega_{\text{gg}}(s, b) \sim T_{\text{gg}}(b) s^{J-1}.$$

Clearly the parameter J is related to the intercept of the Pomeron trajectory $\alpha_P(0)$ of the Regge model. If $J > 1$, the total cross sections grow with energy. Inserting Ω_{gg} in the general expression (11) of the scattering amplitude gives at high energy the following result:

$$\sigma_{\text{tot}} \sim (J-1) (\log s)^2$$

which is formally similar to that obtained in the 'eikonalized' Regge model and in the 'impact picture'.

The main physical point of this model is the connection between the fast rise of the gluonic content of the proton at low x and the growth of σ_{tot} with energy. This same connection has been discussed by other authors (Durand and Pi 1989 and Jenkovszki *et al* 1992).

It has been suggested that a related physical process should be the 'semi-hard' collisions which occur with increasing probability in the energy interval $200 < \sqrt{s} < 900$ GeV as

signalled by the fast rise of the cross section for production of 'minijets' (Ellis and Scott 1989).

Jets having relatively low total transverse momentum ($p_T \sim 5$ GeV) have been called 'minijets'. In the parton model, jets with sizeable transverse momentum result from the elementary process of parton-parton collisions where a transfer of the longitudinal momentum into a transverse component takes place. After the collision the partons 'dress' themselves into observable jets of hadrons. Low- x partons give rise to low- p_T jets. The observed rise of the 'minijet' cross section and of the total cross section, at similar rates in the same energy interval, can be associated to the fast rise of the number of gluons at low x (Dias de Deus and Kwiecinski 1987).

A rather unconventional model which depicts the nucleon as a 'topological soliton', and its applications to high-energy scattering, has been discussed by Islam (1992).

A central issue of present theoretical research (Halzen 1993) is the calculation of the phenomenological properties of the Pomeron within QCD. An important result was obtained by Lipatov (1986 and 1989) who studied a special class of diagrams with multi-gluon exchange and concluded that the Pomeron corresponds to a complicated singularity which may be visualized as a series of poles in the complex angular momentum plane with intercepts becoming higher as the energy increases. This result may be written approximately in the form

$$\alpha_P(0) = 1 + \delta \quad \delta \approx (12/\pi) \alpha_s \log 2 \approx 0.3$$

where α_s is the strong-interaction coupling constant.

A similar calculation was recently performed by Gauron *et al* (1993) for the 'odderon', which plays for the odd signature amplitude F_- , the same role as the Pomeron for the even signature amplitude F_+ . The result is

$$\alpha_{\text{odd}}(0) - 1 > 0.13 [\alpha_P(0) - 1].$$

It should be stressed, however, that these calculations are perturbative. They refer to the region of relatively large momentum transfer (presumably a few GeV^2). As a consequence no definite conclusion can be drawn at present from these results on the low- t region and particularly on the energy dependence of the total cross section and of the total cross section difference between particle and antiparticle.

Among recent developments in the direction of QCD non-perturbative calculations we mention the interesting approach by Nachtmann (1991) and by Dosch *et al* (1992). The interaction of two quarks which is due to the exchange of gluons is actually replaced by the interaction of each quark with an external gluonic field. This effective gluonic potential is supposed to be slowly varying over distances of the order of the effective quark wavelength which is very small because one is dealing with high-energy interactions. This justifies the use of the WKB approximation with the quarks following paths similar to the light-ray paths of the eikonal approximation in optics. The basic quantity of the theory is the vacuum expectation value of the gluon field. Actual calculations of the total cross section and of the slope parameter of forward elastic scattering were performed for meson-meson, meson-baryon and baryon-baryon interactions by Dosch and Ferreira (1993) with encouraging results.

7. Experimental methods

Before discussing the experimental results from the high-energy hadron colliders it is worth describing the experimental techniques used at these machines to measure elastic scattering

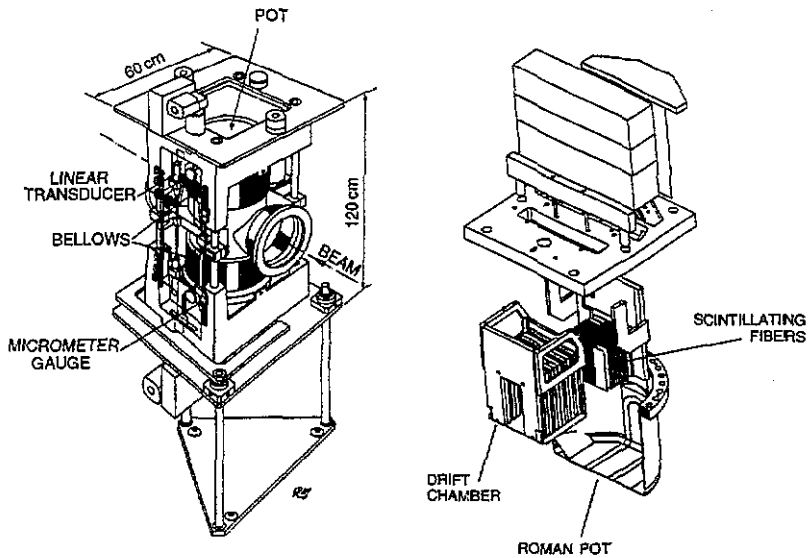


Figure 9. The 'Roman pot' system used at the CERN SPS collider by experiment UA4. A section of the accelerator vacuum chamber is shown together with an exploded view of the detectors.

and the total cross section. These techniques are quite different from those employed with secondary beams at the conventional fixed-target accelerators.

7.1. Elastic scattering

At the hadron colliders the CMS coincides with the laboratory system and measuring elastic scattering is straightforward in principle. One has to detect the two scattered particles demanding back to back angular correlations and requiring no other particles to be present in the final state. Typical scattering angles are, however, quite small (a fraction of mrad) so that the detectors have to be placed very close to the circulating beams.

In practice this is achieved by placing the detectors into movable sections of the vacuum chamber of the accelerator, which have become known as 'Roman pots' and were first used at the CERN ISR (Amaldi *et al* 1973). In its normal position the 'Roman pot' stays in a retreated position leaving the full aperture of the vacuum chamber free for the beam, as required at the injection when the beam is much wide. Once the right energy is attained and the circulating beams are stable, the 'Roman pot' is moved toward the machine axis by compressing the bellows, until the inner edge of the detector reaches a distance of only a few millimeters from the beam. A sketch of the 'Roman pot' system used at the SPS collider is shown in figure 9.

Hadron colliders are usually operated at high luminosity for the search of rare events. To obtain high luminosity, the transverse size of the beam at the crossing point is reduced by the focusing action of quadrupoles. As a consequence the angular divergence of the beams is correspondingly increased so that a large fraction of the scattered particles remain inside the acceptance of the machine itself and are not accessible to detection.

To measure elastic scattering, the opposite scheme is actually required. The beam size at the crossing point is made relatively large while the beam divergence is very small. In practice nearly parallel beams are used. The corresponding loss of luminosity is not a problem because the differential cross section of elastic scattering is large at small t .

The best arrangement is obtained by placing the detectors at a distance from the crossing point equal to one quarter of the period of the betatron oscillations (Haguenauer and Matthiae 1984). In that case optics with parallel-to-point focusing from the crossing point to the detectors is achieved. This has the very convenient property that measuring the particle position at the detector allows the scattering angle to be reconstructed in a straightforward way.

The optical analogue is of course the classical technique of measuring the direction of light rays by means of an optical system with a screen placed at the focal plane.

The detectors which are inserted in the 'Roman pots' are usually designed to accept high rates and have good spatial resolution (about 100 μm). In recent experiments (Amos *et al* 1990a, Augier *et al* 1993b, Abe *et al* 1993) combinations of drift chambers, hodoscopes of scintillating fibres and silicon detectors were used. As an example, the detectors used by Augier *et al* (1993b) at the SPS collider are shown in figure 9.

7.2. Total cross section

At the fixed-target accelerators total hadronic cross sections are measured with the classical transmission technique. The secondary beam is allowed to strike a liquid hydrogen target and from the observed attenuation of the beam itself one obtains the total cross section. Transmission measurements are usually very accurate, at a level of 0.2–0.3%.

At a colliding beam machine, however, different methods have to be used. They are discussed below.

- (1) The first method is based on the definition of total cross section. If the machine luminosity L is known, one makes use of the relationship

$$N_{\text{el}} + N_{\text{inel}} = L \sigma_{\text{tot}} \quad (39)$$

where N_{el} and N_{inel} are the rates of the elastic and inelastic interactions, respectively. This method was used at the ISR (Amendolia *et al* 1973).

- (2) Again if L is known, one may use the optical theorem which relates the total cross section to the imaginary part of the forward amplitude according to (5). The elastic scattering rate dN_{el}/dt is measured at small t and extrapolated to $t = 0$, i.e. to the so-called 'optical point' (Amaldi *et al* 1973). The total cross section is then obtained from the following expression:

$$\left(\frac{dN_{\text{el}}}{dt} \right)_{t=0} = L \left(\frac{d\sigma}{dt} \right)_{t=0} = L \frac{\sigma_{\text{tot}}^2 (1 + \rho^2)}{16\pi}. \quad (40)$$

The parameter ρ is small at high energy, about 0.1–0.2, so that it does not have to be known with high precision to get an accurate value of σ_{tot} .

The main difficulty with methods (1) and (2) is the need of knowing the luminosity. In a fixed-target experiment the effective 'luminosity', defined as the product of the beam intensity (number of incident particles per second) times the number of atoms per square centimetre of the target, can be accurately measured. On the contrary, at a colliding beam machine the measurement of the luminosity is more difficult. In fact what is required is the knowledge of the number of circulating particles and the effective area of the beams at the crossing point. At the ISR the effective beam size was measured with a method invented by Van der Meer (1968) which essentially consists of an 'autoscan' of the beams and reaches a precision of about 1% (Amaldi *et al* 1978).

At the high-energy $\bar{p}p$ colliders, where the beams collide head-on, this method cannot easily be used. The beam size is then measured by a 'wire scan' system (Bossler *et al*

1985) and the luminosity is obtained with a precision of the order of 5%, but the intrinsic systematic errors of the method are difficult to estimate.

- (3) In order to circumvent the problem of measuring the luminosity, the two methods (1) and (2) were combined in a single one, the so-called 'luminosity-independent method'. Combining (39) and (40), the luminosity drops out and we get the following expression:

$$\sigma_{\text{tot}} = \frac{16\pi}{(1 + \rho^2)} \frac{(dN_{\text{el}}/dt)_{t=0}}{N_{\text{el}} + N_{\text{in}}}. \quad (41)$$

This 'luminosity-independent' method allows in principle a better control of the systematic effects. It was used at the ISR by Amaldi *et al* (1978), at the SPS collider by Bozzo *et al* (1984c) and at the Tevatron by Amos *et al* (1990a) and by Abe *et al* (1993).

- (4) The last method relies on the measurement of Coulomb scattering (a process whose cross section is well known) to normalize the observed t -distribution dN_{el}/dt and get the differential cross section $d\sigma/dt$. Because of its $1/\theta^4$ distribution, Coulomb scattering becomes dominant over hadronic scattering only at very small momentum transfer. In fact the two processes have the same probability when the momentum transfer is

$$t_0 \simeq \frac{8\pi\alpha}{\sigma_{\text{tot}}} \quad (42)$$

where α is the fine structure constant. Numerically, at high energy, $t_0 \simeq 10^{-3} \text{ GeV}^2$.

These four methods for measuring the total cross section are not straightforward. As a consequence the results are affected by errors of few percent, quite larger than for the fixed-target experiments.

7.3. The real part in the forward direction

The real part of the hadronic amplitude is obtained by observing the interference with the Coulomb amplitude which is known. This standard technique, however, provides a measurement of the real part only for those values of the momentum transfer where the two amplitudes are comparable in magnitude, i.e. for $t \approx t_0$. Thus in practice the real part can be measured only in the forward direction. To account for both, hadronic and Coulomb scattering, the differential cross section is written as

$$\frac{d\sigma}{dt} = \frac{16\pi}{s^2} |F_{\text{C}} e^{(\mp i\alpha\phi)} + F_{\text{h}}|^2. \quad (43)$$

The Coulomb amplitude F_{C} is given by

$$F_{\text{C}} = \pm \frac{1}{2} \alpha s \frac{G^2(t)}{|t|}$$

where $G(t)$ is the proton electromagnetic form factor. The upper and lower sign refer to $\bar{p}p$ and pp scattering, respectively. For the hadronic amplitude the following low- t parametrization is normally used:

$$F_{\text{h}} = \frac{s}{16\pi} \sigma_{\text{tot}} (\rho + i) e^{Bt/2}$$

where ρ is the ratio of the real to the imaginary part in the forward direction. The interference term in (43) is proportional to the quantity $(\rho \pm \alpha\phi)$.

The relative Coulomb-hadronic phase $\alpha\phi$, first calculated by Bethe (1958) for a potential scattering model, was afterwards discussed by various authors (West and Yennie 1968,

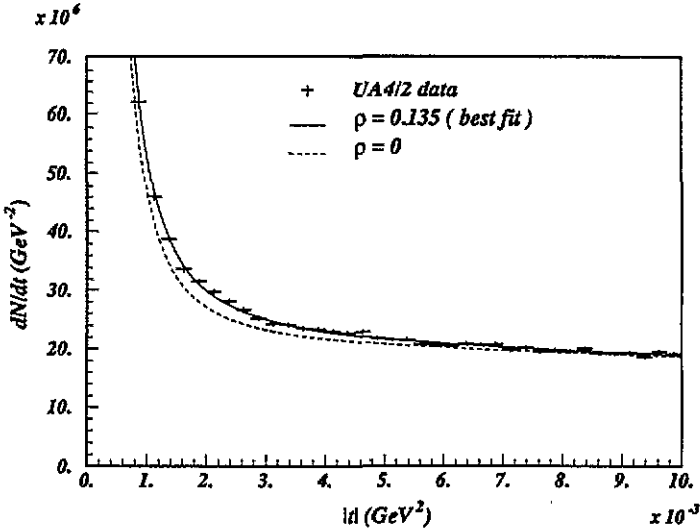


Figure 10. The t -distribution of $\bar{p}p$ elastic scattering at $\sqrt{s} = 540$ GeV in the region of the Coulomb interference (Augier *et al* 1993b).

Buttimore *et al* 1978, Cahn 1982, Kundrat and Lokajicek 1993). A reasonably good approximation for $B = 15 \text{ GeV}^{-2}$ is

$$\phi = \log \frac{0.07}{|t|} - 0.577.$$

Numerically $\alpha\phi \simeq 0.027$ at $t = t_0$.

As an example, recent data in the Coulomb region from the SPS collider (Augier *et al* 1993b) are shown in figure 10. The rise at very low t is due to Coulomb scattering. The best fit which gives $\rho = 0.135$ is represented by the full curve while the broken curve indicates the result which would have been obtained for $\rho = 0$. These data supersede a previous, less accurate measurement (Bernard *et al* 1987b).

8. Experimental results on σ_{tot} and $d\sigma/dt$

Results from fixed-target experiments are limited to CMS energies less than about 20 GeV. The data at higher energies are from the colliding beam accelerators. The CERN ISR have provided pp and $\bar{p}p$ collisions in the energy interval $\sqrt{s} \simeq 20\text{--}60$ GeV. The SPS collider at CERN and the Tevatron at Fermilab provide $\bar{p}p$ collisions in the range $\sqrt{s} \simeq 0.5\text{--}1.8$ TeV.

8.1. Total cross section and real part

Measurements of the total cross section and of the parameter ρ are discussed together in this section because they are correlated by the dispersion relations.

It has been observed that the $\bar{p}p$ and pp total cross sections tend to become equal as the energy increases. Data on the total cross section difference $\Delta\sigma_{\text{tot}} = \sigma_{\text{tot}}(\bar{p}p) - \sigma_{\text{tot}}(pp)$ from the ISR (Amos *et al* 1985 and Carboni *et al* 1985) are shown in figure 11 together with measurements at lower energy. The full line in figure 11 represents the result of a power-law fit which gives $\Delta\sigma_{\text{tot}} \sim s^{-0.56}$. A power law with exponent close to $\frac{1}{2}$ is indeed expected in the Regge model for exchange of the dominant odd-signature trajectories. Clearly the

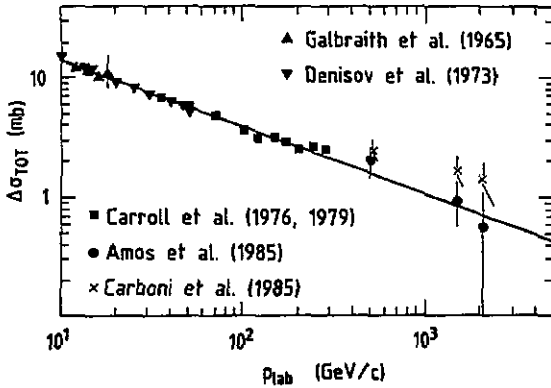


Figure 11. The total cross section difference $\Delta\sigma_{\text{tot}} = \sigma_{\text{tot}}(\bar{p}p) - \sigma_{\text{tot}}(pp)$ as a function of energy.

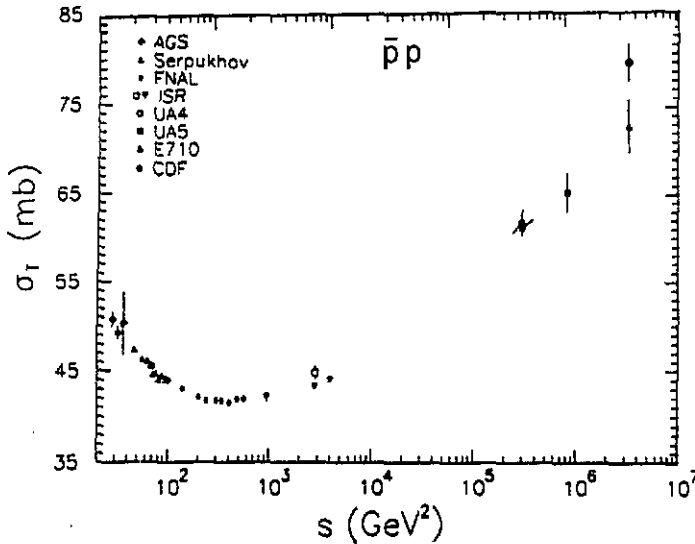


Figure 12. The proton-antiproton total cross section as a function of energy.

experimental results on $\Delta\sigma_{\text{tot}}$ are consistent with the assumption that the amplitude which is odd under crossing becomes negligible at high energy at least in the forward direction.

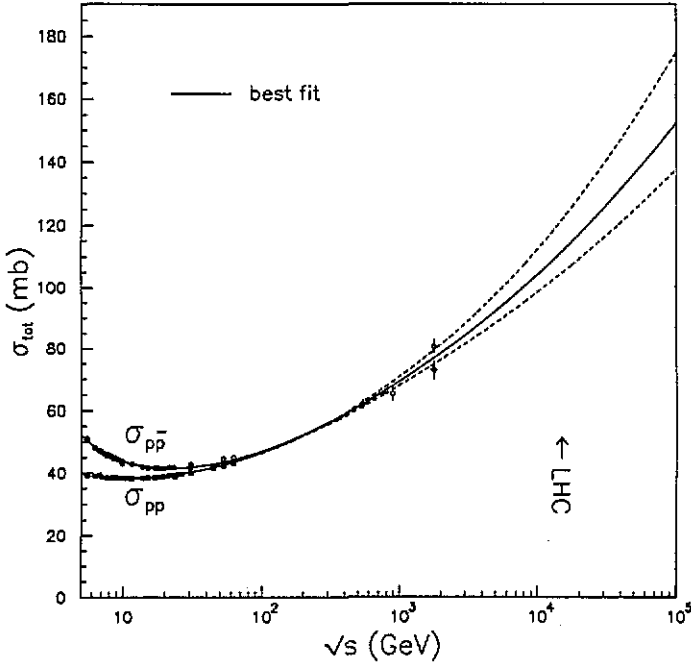
A compilation of the data on the proton-antiproton total cross section is presented in figure 12. The cross section grows by nearly a factor of two from the ISR up to the Tevatron energy. The experimental results in the high-energy range, $0.546 < \sqrt{s} < 1.8$ TeV are collected in table 1.

The recent data of the CDF experiment at $\sqrt{s} = 546$ GeV agrees well with the earlier UA4 measurement at the same energy. However, the CDF result at 1.8 TeV is definitely higher than the previous measurement by the E710 experiment. Both experiments have employed the same technique, the luminosity-independent method, so that the origin of the discrepancy is at present unclear.

The energy dependence of the total cross section can be studied in a model-independent way with the help of the dispersion relations. The energy dependence of σ_{tot} is described by a suitable function containing free parameters which are determined by fitting the $\bar{p}p$ and pp data on σ_{tot} and ρ . A simple but effective parametrization, first used by Amaldi *et*

Table 1. Data on the $\bar{p}p$ total cross section from the high-energy colliders.

\sqrt{s} (TeV)	σ_{tot} (mb)	Experiment
0.546	62.2 ± 1.5	UA4 (Bozzo <i>et al</i> 1984c)
	61.3 ± 1.0	CDF (Abe <i>et al</i> 1993)
0.90	65.3 ± 1.7	UA5 (Alier <i>et al</i> 1986)
1.8	72.8 ± 3.1	E710 (Amos <i>et al</i> 1992)
	80.0 ± 2.2	CDF (Abe <i>et al</i> 1993)

Figure 13. Total cross sections of $\bar{p}p$ and pp . The result of the dispersion relation fit of Augier *et al* (1993a) is also shown. The broken curves indicate the uncertainty region of the fit.

al (1977) is the following:

$$\sigma_{\text{tot}} = A_1(s/s_0)^{-n_1} \mp A_2(s/s_0)^{-n_2} + C_0 + C_2 (\log s/s_0)^\gamma \quad (44)$$

where the upper and the lower sign refer to pp and $\bar{p}p$, respectively. The power terms in (44) are needed to reproduce the low-energy data while a logarithmic form is taken for the high-energy behaviour. The amplitude odd under crossing is assumed to vanish asymptotically in accordance with present data. The scale factor s_0 is usually taken equal to 1 GeV^2 .

The principal aim is to derive from the data the value of the parameter γ which controls the high-energy behaviour of the cross section and to make predictions at energies above those of the present accelerators. Earlier fits (Amaldi *et al* 1977, and Amos *et al* 1985) on data up to $\sqrt{s} = 53 \text{ GeV}$ gave the result $\gamma \approx 2$. This conclusion is confirmed by a recent and similar analysis by Augier *et al* (1993a), using a data sample in the range of energy $5 \leq \sqrt{s} \leq 546 \text{ GeV}$ which includes a new, accurate measurement of ρ at the SPS collider (Augier *et al* 1993b). The result of the best fit which gives $\gamma = 2.2 \pm 0.3$ is shown in

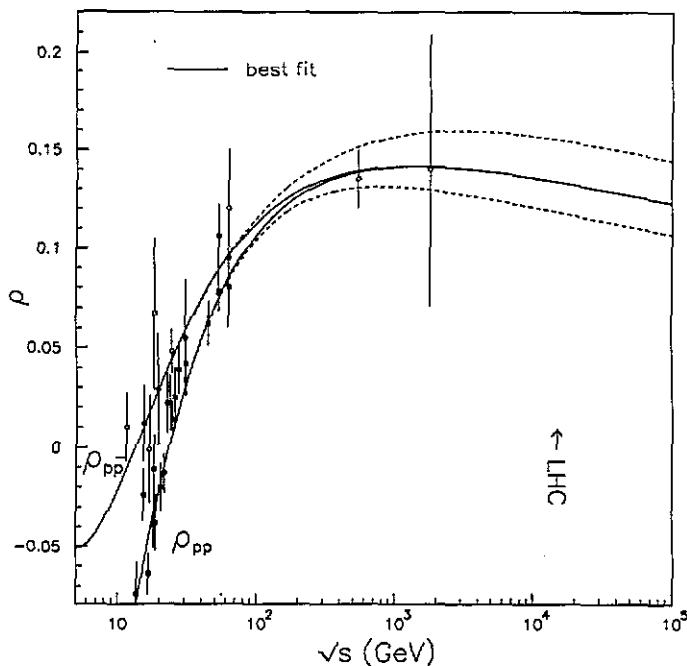


Figure 14. Measurements of the ρ parameter for $\bar{p}p$ and pp scattering are shown together with the result of the dispersion relation fit of Augier *et al* (1993a). The broken curves indicate the uncertainty of the fit.

figure 13 together with the experimental data.

In spite of the large error which is due to the strong correlation existing between the different parameters in (44), the result of this analysis clearly favours the $(\log s)^2$ dependence. This behaviour has been often referred to as 'qualitative' saturation of the Froissart–Martin bound in the sense that it corresponds to the maximum rate of rise with energy which is allowed by analyticity and unitarity, but numerically actual data lie much below the absolute value of the bound itself.

The fit by Augier *et al* (1993a) provides predictions at higher energies, in particular at the future accelerator LHC ($\sqrt{s} = 16$ TeV). The numerical values obtained from the fit are given in table 2 together with the corresponding uncertainties.

The experimental results at $\sqrt{s} = 546$ GeV are well reproduced by the best fit. The prediction of the fit at $\sqrt{s} = 1.8$ TeV lies in between the results reported by the two Fermilab experiments E710 and CDF.

Table 2. Results of the dispersions relation fit of Augier *et al* (1993a) .

\sqrt{s} (TeV)	σ_{tot} (mb)
0.546	61.8 ± 0.7
0.90	67.5 ± 1.3
1.8	76.5 ± 2.3
16.0	111.0 ± 8.0
40.0	130.0 ± 13.0

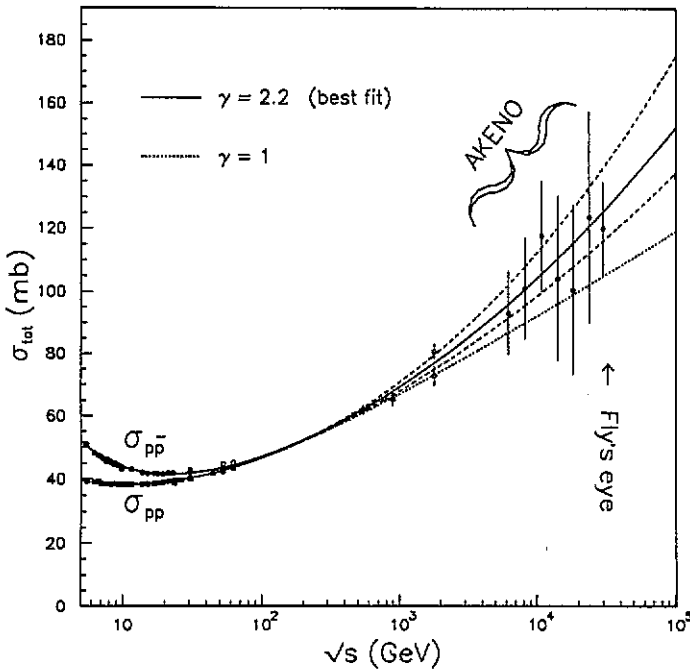


Figure 15. Cosmic-rays results are shown together with the total cross sections measured at the accelerators. Full and broken curves refer to the dispersion relation analysis as in figure 13. The dotted curve indicates the linear rise with $\log s$.

A compilation of data on the parameter ρ for $\bar{p}p$ and pp scattering is presented in figure 14 together with the dispersion relation fit of Augier *et al* (1993a). The energy dependence of ρ clearly follows the expected trend, discussed in section 3, with a broad maximum in the few TeV region followed by a gentle decrease at higher energy.

Information on the total cross section of protons at very high energies, above those accessible with present accelerators, is provided by the study of the interactions of primary cosmic rays in the atmosphere. From the measurement of the absorption length of the incoming protons in air, the total cross section of protons on nucleons can be derived by means of the Glauber model (1959). In spite of their large systematic uncertainties, these results are meaningful because extend up to CMS energies as large as 30 TeV. The data reported from the 'fly's eye' detector (Baltrusaitis *et al* 1984) and from the Akeno observatory (Honda *et al* 1993) are shown in figure 15 together with the accelerator results. The cosmic rays data support the conclusion of the dispersion relation analysis by Augier *et al* (1993a) favouring the $(\log s)^2$ behaviour with respect to the linear rise with $\log s$.

8.2. The ratio of the elastic to the total cross section

The ratio of the elastic to the total cross section, σ_{el}/σ_{tot} , is known to decrease at low energy and then reach a constant value in the range of energy of the ISR. For pp interactions accurate measurements are available which give as average value $\sigma_{el}/\sigma_{tot} = 0.175$ between $\sqrt{s} = 23$ GeV and $\sqrt{s} = 62$ GeV. The $\bar{p}p$ data at the same energies have larger errors but are consistent with this value. These results led to the notion of 'geometrical scaling' (section 3.1) which predicted that the ratio σ_{el}/σ_{tot} would be energy-independent.

However, more recent results from the SPS and the Tevatron colliders (Bozzo *et al* 1984c, Amos *et al* 1990a and Abe *et al* 1993) have shown that at energies above those of the ISR, this ratio increases although at a very slow rate. This means that the colliding particles become effectively more 'opaque' at high energy in agreement with the prediction of the 'impact picture' (Bourrely *et al* 1990). A compilation of data on the ratio of the elastic to the total cross section for $\bar{p}p$ scattering is shown in figure 16.

8.3. The forward peak

At high energy the t -distribution of elastic scattering exhibits a forward peak, often called the 'diffraction peak', with an approximately exponential form which is followed, at $-t \sim 1 \text{ GeV}^2$, by a structure with a dip-bump or dip-shoulder shape. At still higher momentum transfer the differential cross section falls off much more gently. This general behaviour is illustrated in figure 17 where data on pp elastic scattering in the energy region of the ISR are presented.

At low momentum transfer, $-t < 0.1 \text{ GeV}^2$, the differential cross section is well described by the simple exponential e^{Bt} . As already noted in section 3.1, this implies that the relation, $\sigma_{\text{tot}}/B = 16\pi\sigma_{\text{el}}/\sigma_{\text{tot}}$, is approximately correct. Therefore, if the ratio $\sigma_{\text{el}}/\sigma_{\text{tot}}$ is constant, the forward-slope parameter B will have the same energy dependence as the total cross section.

The ratio $\sigma_{\text{el}}/\sigma_{\text{tot}}$ is actually increasing, although slowly, with energy, and we then expect the forward slope B to increase with energy at a rate which is slightly less fast than that of the total cross section. This is indeed the case as shown in figure 18. The data are consistent with a $\log s$ rise which is in fact expected in the Regge model (section 4) which predicts a forward slope of the form $B(s) = B_0 + 2\alpha'_p \log s$. Numerically the effective slope of the Pomeron trajectory turns out to be $\alpha'_p \approx 0.25 \text{ GeV}^{-2}$.

A direct comparison of pp and $\bar{p}p$ elastic scattering in the region of the diffraction peak was performed at the ISR measuring both reactions with the same experimental apparatus (Breakstone *et al* 1984a). As shown in figure 19, the ratio of the slope parameters $B(\bar{p}p)/B(pp)$ decreases with energy and, within the (small) experimental errors, becomes equal to 1 at $\sqrt{s} = 62 \text{ GeV}$. This indicates that the theorem (27) on the asymptotic equality of the slopes for $\bar{p}p$ and pp scattering is already verified at the 1% level at the top ISR energy.

A closer look at the shape of the forward diffraction peak reveals that in general it is not a simple exponential. Accurate measurements on proton-proton scattering at the ISR (Barbiellini *et al* 1972), have shown that the t -dependence of the differential cross section is steeper near the forward direction, i.e. the t -distribution shows a positive curvature (figure 20). The local slope parameter $B(t)$, derived by fitting the data with the exponential e^{Bt} in different regions of t , decreases by about 2 units of GeV^{-2} when one moves away from the forward direction.

A similar effect was also observed at the SPS collider (Bozzo *et al* 1984b) as shown in figure 21. At the Tevatron collider, on the contrary, the data by Amos *et al* (1990b) show a simple exponential shape down to $-t = 0.5 \text{ GeV}^2$ (figure 22).

A summary of the experimental information on the shape of the forward peak is presented in figure 23 where the local slope parameter $B(t)$ is plotted as a function of t for pp and $\bar{p}p$ scattering at different energies. The horizontal bar in figure 23 indicates the interval in t where the exponential fit was actually performed.

This change with energy of the shape of the diffraction peak is actually expected in the diffraction models discussed in section 5 (Bourrely *et al* 1988 and Barshay *et al* 1992).

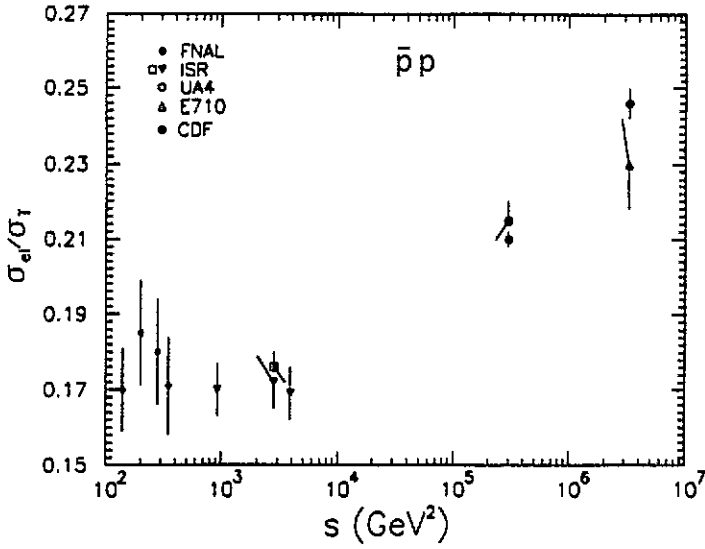


Figure 16. The ratio of the elastic to the total cross section for $\bar{p}p$ interactions as a function of energy.

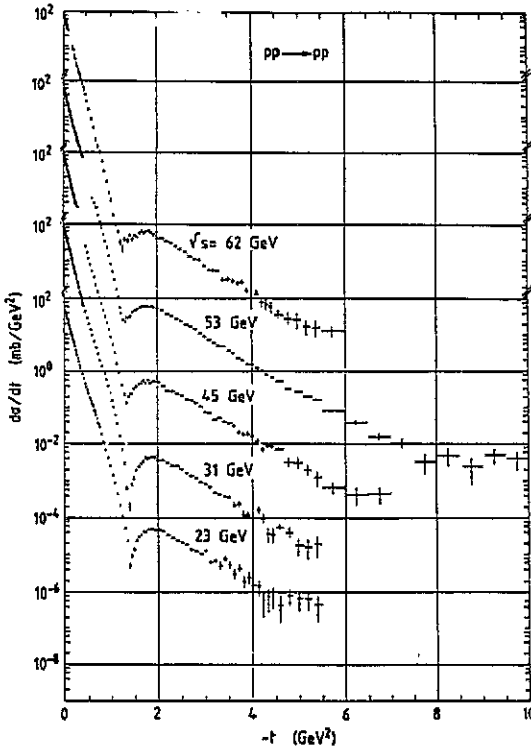


Figure 17. Proton-proton elastic scattering as measured at the CERN ISR. The differential cross section at different CMS energies from 23 GeV up to 62 GeV is shown as a function of the momentum transfer.

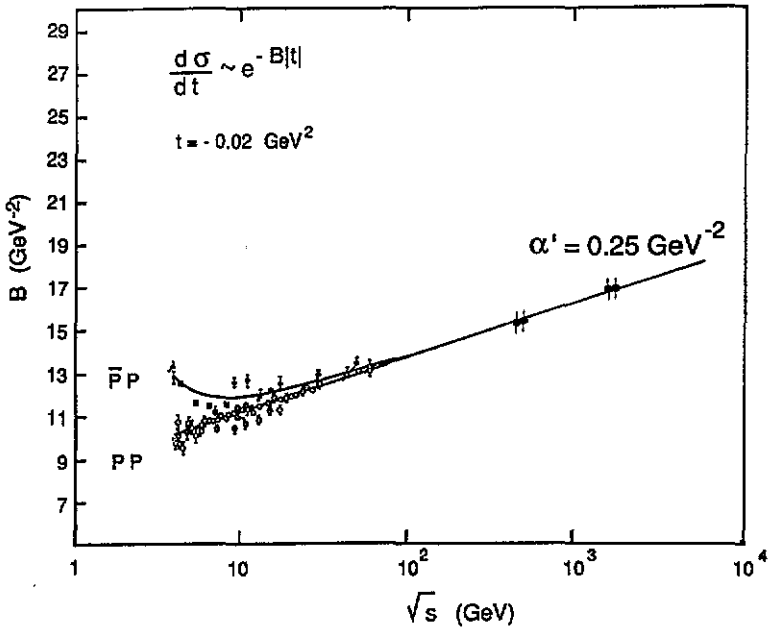


Figure 18. The forward-slope parameter B for $\bar{p}p$ and pp elastic scattering. The full curve refers to the Pomeron trajectory of the Regge model.

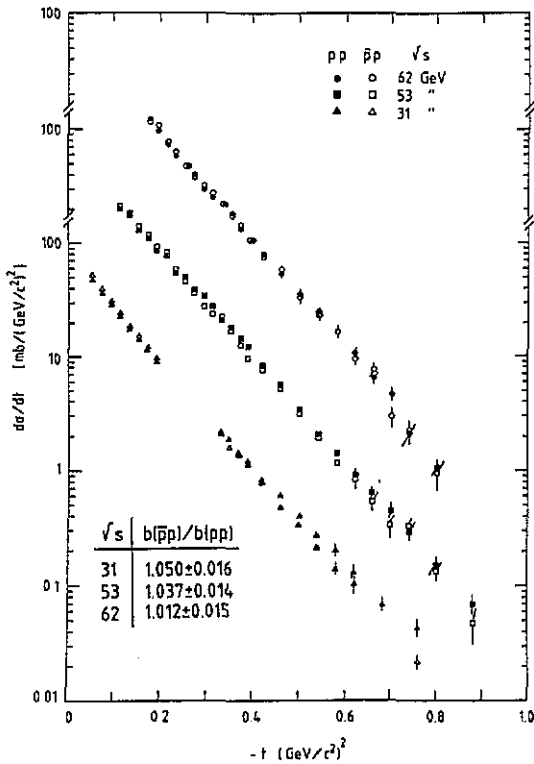


Figure 19. Comparison of $\bar{p}p$ and pp elastic scattering at low momentum transfer in the energy region of the ISR (Breakstone *et al* 1984a).

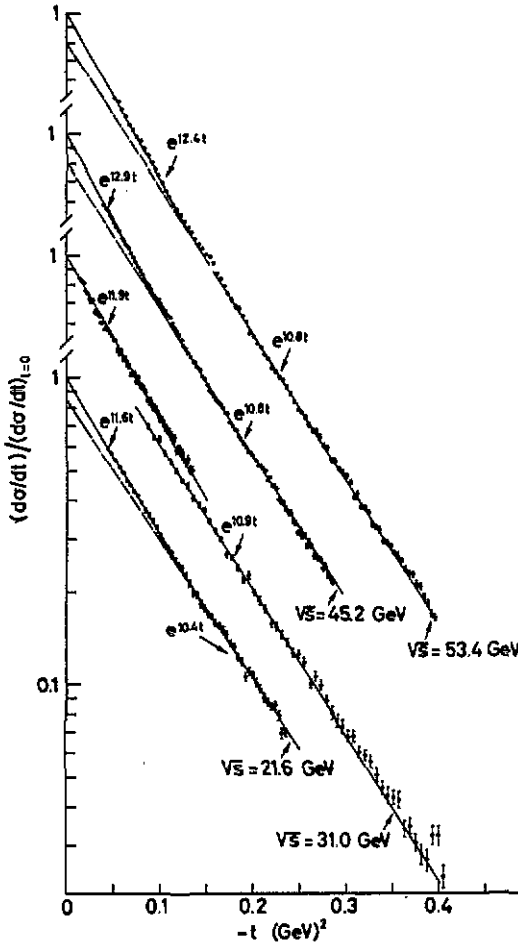


Figure 20. The shape of the forward peak in pp elastic scattering at the ISR energies (Barbiellini *et al* 1972).

Asymptotically these models predict for elastic scattering a form equal or similar to the Fraunhofer formula (34) which has a negative curvature. At low energies the shape of the t -distribution is determined by the proton electromagnetic form factor which has a positive curvature. Therefore the curvature will change from positive to negative at some finite energy. This feature of the data can also be reproduced in the Regge approach, as due to the interplay of the two amplitudes for single and double Pomeron exchange which have different energy and momentum-transfer dependence.

8.4. The dip-shoulder region

The proton-proton data from the ISR show a clear structure in the momentum-transfer region, $1 \leq -t \leq 2 \text{ GeV}^2$, with a shape of a dip followed by a broad maximum, which is typical of a diffraction pattern (figure 17). Such a structure had in fact been predicted (Chou and Yang 1968) several years before the measurements could actually be performed. The momentum transfer at the position of the dip varies proportionally to $1/\sigma_{\text{tot}}$, as expected in the diffraction models.

The depth of the minimum is not the same at the different energies. Formally, the minimum of the diffraction pattern corresponds to a zero of the imaginary part of the

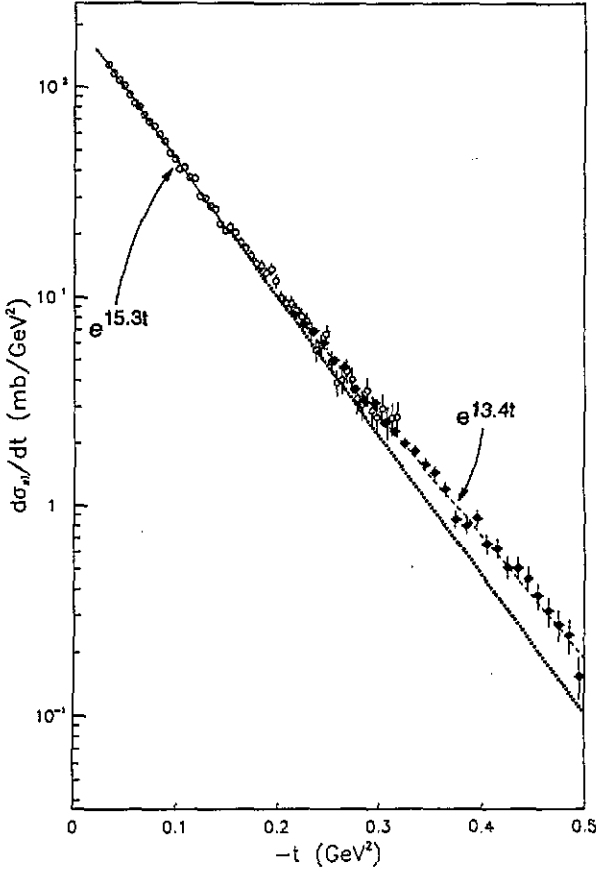


Figure 21. The shape of the forward peak in $\bar{p}p$ elastic scattering at $\sqrt{s} = 546$ GeV from the UA4 experiment of Bozzo *et al* (1984b).

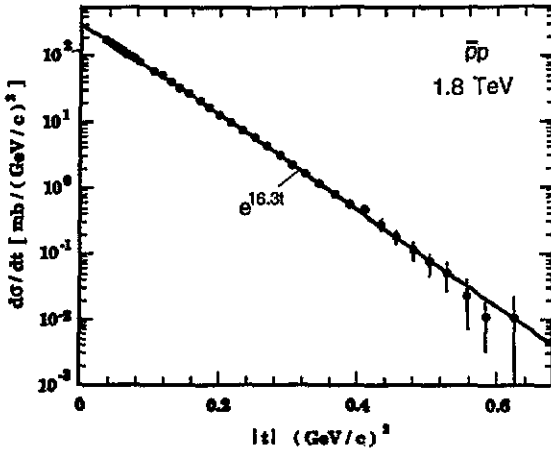


Figure 22. The forward elastic peak of $\bar{p}p$ scattering at $\sqrt{s} = 1.8$ TeV from the E710 experiment at the Fermilab Tevatron (Amos *et al* 1990b).

scattering amplitude, so that the level of the cross section at the dip is determined by the value of the real part which varies with energy.

Current models are able to reproduce the proton-proton scattering data quite well. As examples we show in figure 24 the results of the Regge model of Donnachie and Landshoff (1986) and in figure 25 the results of the impact picture of Bourrely *et al* (1984). It should

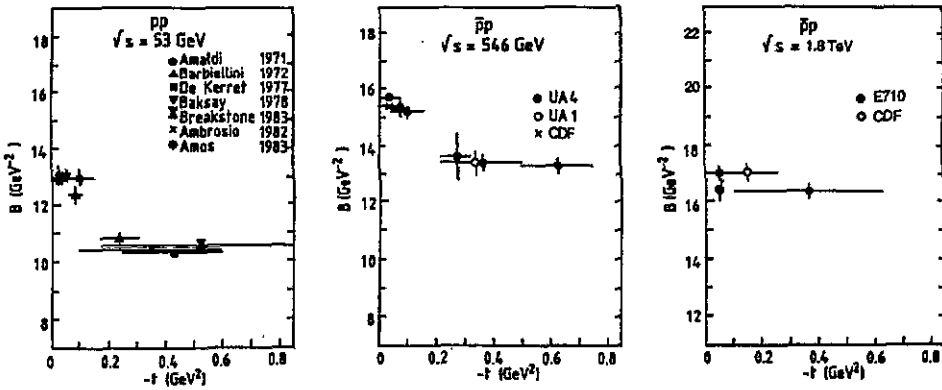


Figure 23. The local slope parameter $B(t)$ is plotted as a function of t for pp scattering at $\sqrt{s} = 53 \text{ GeV}$ and for $\bar{p}p$ scattering at $\sqrt{s} = 546 \text{ GeV}$ and $\sqrt{s} = 1.8 \text{ TeV}$.

be noted that in the impact picture there is no basic difference between $\bar{p}p$ and pp in the dip region at high energy.

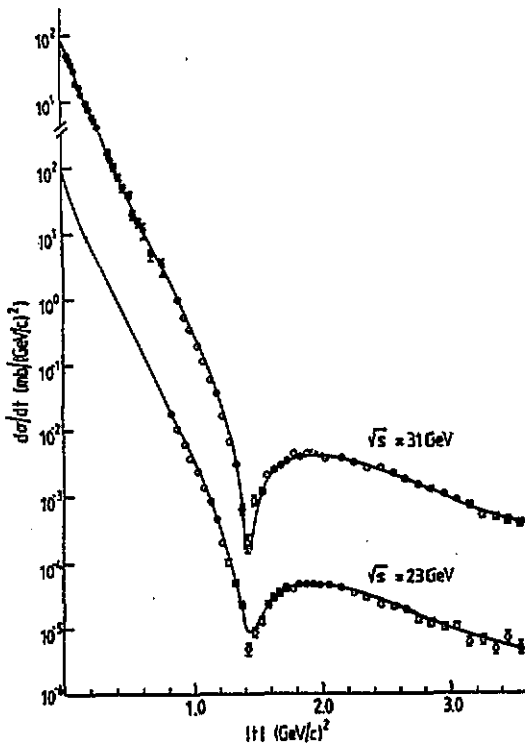


Figure 24. The differential cross section of pp elastic scattering at $\sqrt{s} = 23$ and 31 GeV is shown together with the results of the Regge model of Donnachie and Landshoff (1986) represented by the full curves.

In fact, when measurements on $\bar{p}p$ scattering were performed, it was found that there is a difference between $\bar{p}p$ and pp in the region of the dip as shown in figure 26 where the $\bar{p}p$ data at $\sqrt{s} = 53 \text{ GeV}$ by Breakstone *et al* (1985) are plotted together with the earlier results on pp scattering by Nagy *et al* (1979) at the same energy. The $\bar{p}p$ data do not show a dip but only a break followed by a shoulder.

This effect is explained by the model of Donnachie and Landshoff (1983 and 1986) as due to the presence of the three-gluon exchange mechanism which will be discussed in more

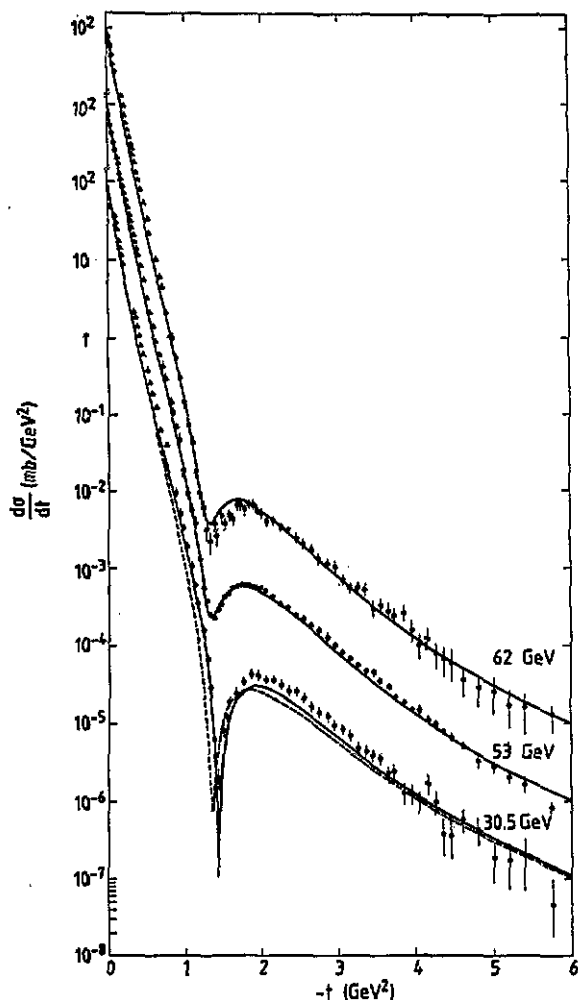


Figure 25. The differential cross section of pp elastic scattering at three different energies is shown together with the results of the impact picture of Bourrely *et al* (1984) represented by the full curves. The broken curve is a prediction for $\bar{p}p$ scattering.

detail in section 8.5. The amplitude of this process has different signs for pp and for $\bar{p}p$ scattering. Its interference with the complex amplitude which describes the diffraction peak is destructive in pp scattering, thus producing a dip, but, on the contrary, is constructive for $\bar{p}p$ giving rise only to a break. The experimental results on the ratio of the $\bar{p}p$ to pp differential cross section at $\sqrt{s} = 53$ GeV in the region of the dip are shown in figure 27 together with the prediction of this model.

The measurements of $\bar{p}p$ elastic scattering at the SPS collider by the UA4 experiment (Bozzo *et al* 1985) are shown in figure 28 together with previous pp results at $\sqrt{s} = 53$ GeV. Also, these $\bar{p}p$ data do not show a dip but only a break followed by a shoulder in agreement with the expectations of the three-gluon interference model.

An interesting feature of the UA4 results is that the level of the differential cross section on the shoulder is more than one order of magnitude above the ISR data. This effect was qualitatively predicted by the 'geometrical model' as shown in figure 5. More elaborate models as the impact picture of Bourrely *et al* (1988) or the 'eikonalized' Regge models are able to reproduce this feature of the data quite accurately. In these models the asymptotic limit of the differential cross section corresponds to the Fraunhofer diffraction by a fully

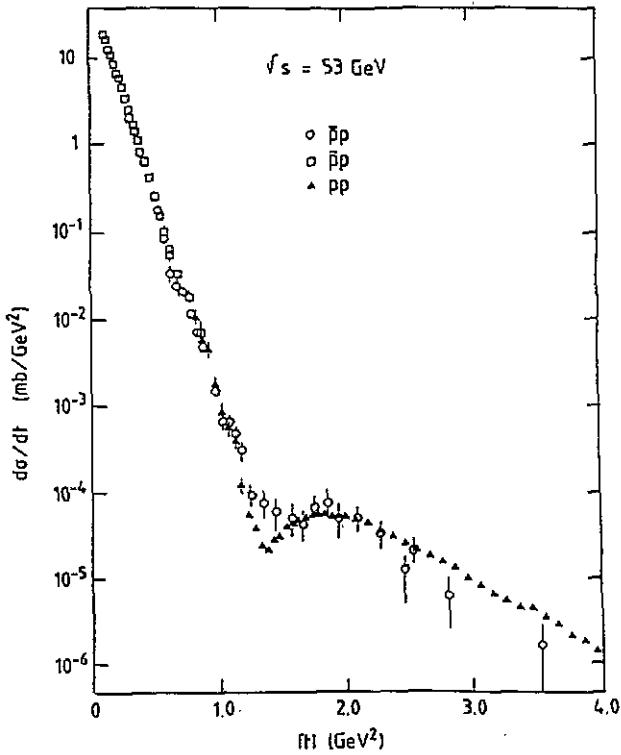


Figure 26. Differential cross section of proton-proton and proton-antiproton elastic scattering at $\sqrt{s} = 53$ GeV.

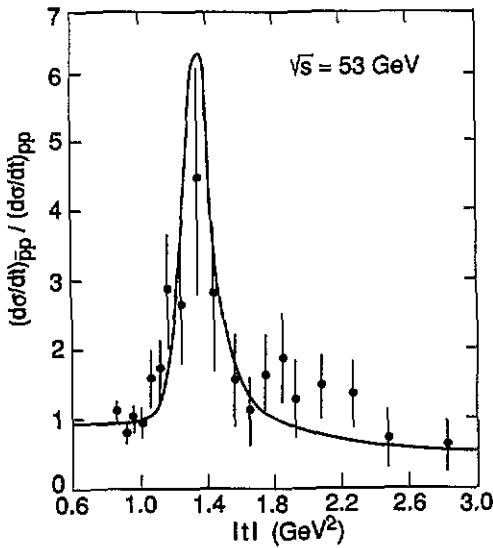


Figure 27. The ratio of the differential cross sections of $\bar{p}p$ to pp elastic scattering at $\sqrt{s} = 53$ GeV in the region of the structure is compared with the prediction of the three-gluon interference model (Landshoff 1991).

absorbing disk (34). In this limiting case the ratio

$$\frac{(\frac{d\sigma}{dt})_{2nd\ max}}{(\frac{d\sigma}{dt})_{t=0}} \quad (45)$$

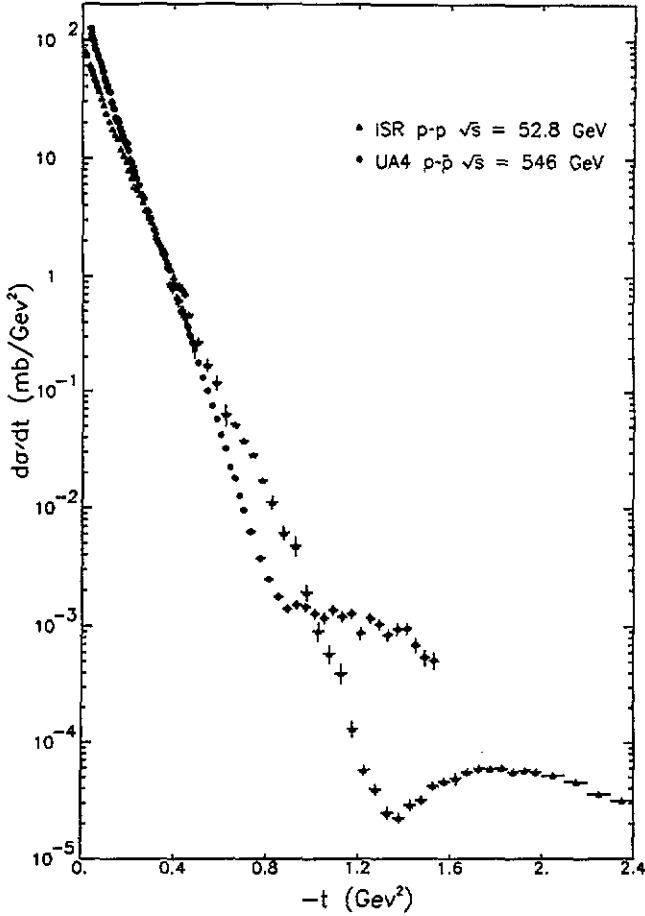


Figure 28. Differential cross section of pp elastic scattering at $\sqrt{s} = 53$ GeV and of $\bar{p}p$ scattering at $\sqrt{s} = 546$ GeV.

would take the value 0.0175. Experimentally the ratio (45) is about 10^{-6} at the ISR and about 10^{-5} at the SPS collider energy.

The ‘eikonalized’ Regge model of Covolan *et al* (1992) is able to reproduce the shape of the differential cross section quite well up to the maximum energy of the Tevatron. The results of this model for $\bar{p}p$ scattering at $\sqrt{s} = 53, 546$ and 630 GeV are shown in figure 29 together with the experimental data from Breakstone *et al* (1984a and 1985), Bozzo *et al* (1985) and Bernard *et al* (1986b). The Tevatron data from Amos *et al* (1990b) and the result of the model at $\sqrt{s} = 1.8$ TeV are shown in figure 30.

8.5. The large-momentum-transfer region

In the region of momentum transfer beyond the structure, the differential cross section shows a rather gentle fall off, much less fast than in the forward peak. This is particularly evident in the pp data at $\sqrt{s} = 53$ GeV (see figure 17) which extend up to $-t \simeq 10$ GeV². Unfortunately no data are available for the $\bar{p}p$ channel at these high values of the momentum transfer because of the limited luminosity of the $\bar{p}p$ colliders.

The analysis of the large- t results shows that at fixed t the cross section is a fast

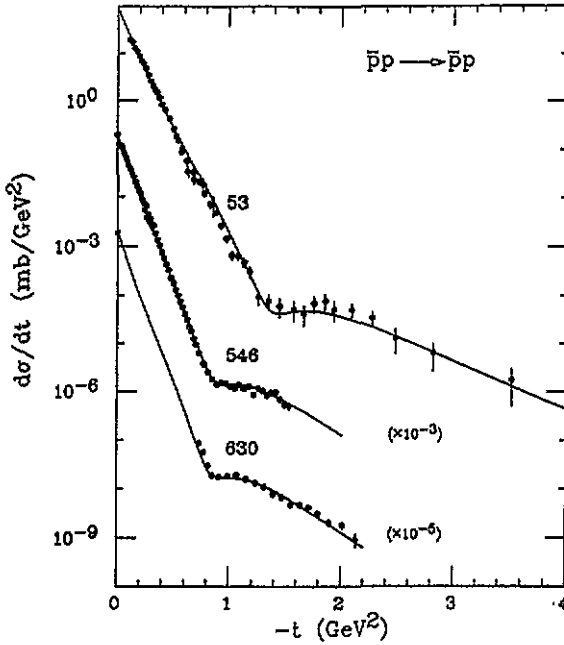


Figure 29. The results of the Regge model by Covolan *et al* (1992) on $\bar{p}p$ elastic scattering at the ISR and SPS collider energies are shown together with the experimental data.

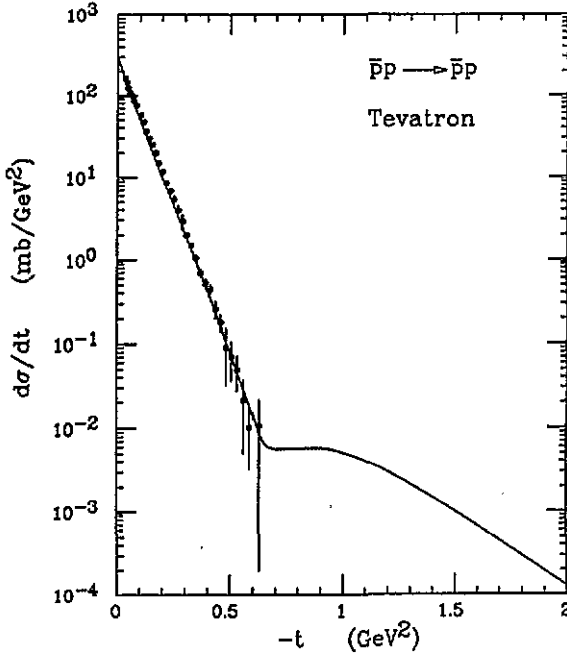


Figure 30. The result of the Regge model by Covolan *et al* (1992) at the Tevatron energy ($\sqrt{s} = 1.8$ TeV) is shown together with the experimental data.

decreasing function of the collision energy up to $\sqrt{s} \sim 10$ GeV and then seems to flatten off and remain constant. When energy and momentum transfer are sufficiently large, the

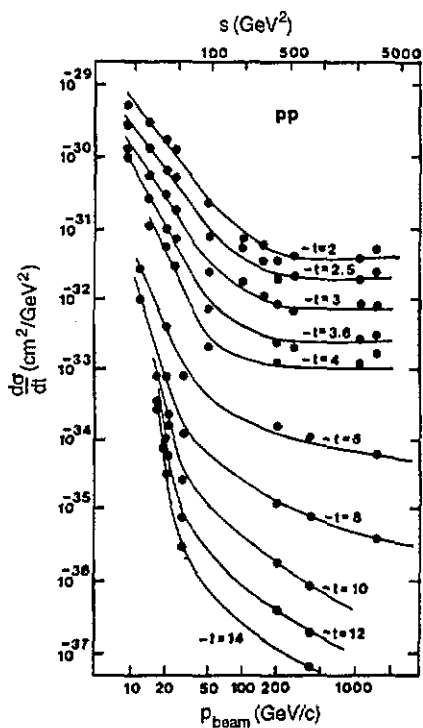


Figure 31. Proton-proton elastic scattering at large t . Energy dependence of the differential cross section at fixed t .

THREE - GLUON EXCHANGE

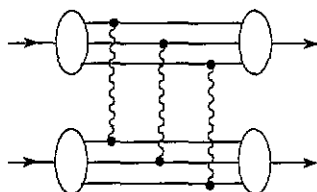


Figure 32. The three-gluon exchange diagram for large- t proton-proton elastic scattering in the model of Donnachie and Landshoff (1979).

differential cross section becomes only a function of t and no longer of s , as shown in figure 31.

This feature of the data suggests the onset of a specific dynamic mechanism which, according to Donnachie and Landshoff (1979), is provided by the exchange of three gluons between the valence quarks of the two colliding protons (figure 32). In this model the proton is regarded as a three-quark state. In the elastic collision each quark in one proton scatters on one of the quarks of the other proton so that after the three elementary scattering processes of the constituent quarks, each triplet of quarks is again moving almost in the same direction and may thus recombine to form a proton.

The cross section of the three-gluon exchange diagram can be approximately calculated and in the limit of large s and t , but $-t \ll s$, is independent of s and decreases as the eighth power of t ,

$$\frac{d\sigma}{dt} = C \frac{1}{t^8}. \tag{46}$$

Unfortunately the theory at present cannot provide a reliable estimate of the normalization factor C .

The t -dependence of the data at fixed energy indeed follows the theoretical expectation quite well as shown in figure 33 where pp data at $\sqrt{s} \simeq 25$ GeV and 53 GeV are plotted.

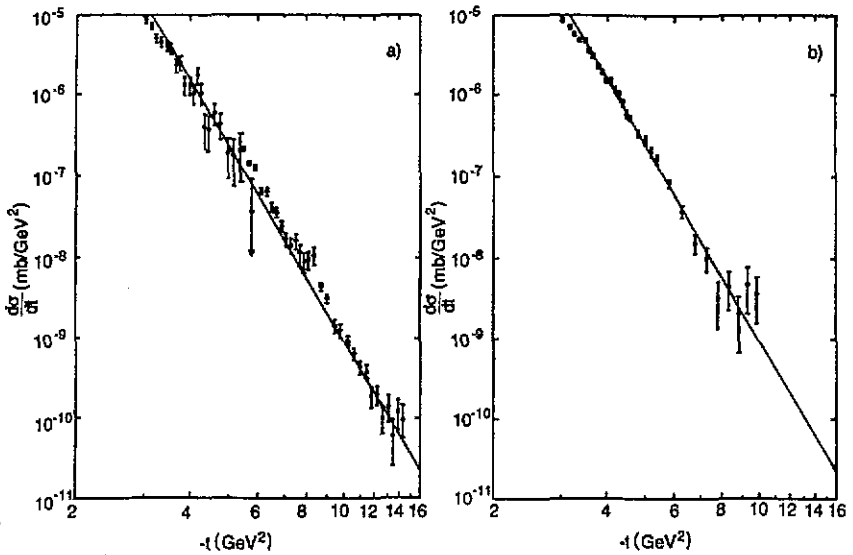


Figure 33. Proton-proton elastic scattering at large t from Faissler *et al* (1981) and Nagy *et al* (1979) (a) Data at $\sqrt{s} \approx 25$ GeV (b) Data at $\sqrt{s} = 53$ GeV. The full lines correspond to $d\sigma/dt = 0.09/t^8$.

The full lines in figure 33 correspond to the numerical value $C = 0.09 \text{ mb GeV}^{14}$.

It is interesting to note that the spin of the gluons plays a crucial role in this context. In fact if gluons had spin 0 instead of 1, the s and t dependence of the differential cross section would be completely different. The theory predicts $d\sigma/dt \sim s^{-6}t^{-2}$, which is clearly in disagreement with the experimental results.

If the dominant mechanism at large momentum transfer is again the three-gluon exchange at higher energies, the t -distribution should be smooth, without structure. The 'impact picture', on the contrary, predicts the appearance of a new structure with at least a new diffraction minimum.

9. Diffraction dissociation

9.1. General features

The process of diffraction dissociation is closely related to elastic scattering. It may be regarded as a two-body reaction



where particle a is excited to a system X which then decays, or fragments, in a certain number of stable particles. Reaction (47) is also known as 'single diffraction' while the name 'double diffraction' is reserved to the process where particle b is also excited.

To be diffractively produced the system X must have the same intrinsic quantum numbers as the incoming particle a , i.e. same charge, isospin, strangeness, etc, while spin and parity may be different because some orbital angular momentum can be transferred to X in the collision. In the exclusive reactions where X is experimentally identified as a known resonance, it has always been observed that if the previous condition is verified, then the differential cross section exhibits a sharp forward peak with a slope parameter similar to

that of elastic scattering. In addition, the production cross section of these resonances has energy dependence similar to that of the elastic cross section.

In a high-energy collision the mass M of the system X may take quite large values with a limitation which is imposed by the coherence condition as was first remarked by Good and Walker (1960). If p_0 is the laboratory momentum of the incoming particle a , the momentum p of the system X , when produced in the forward direction, is

$$p \simeq p_0 - (M^2 - m_a^2)/2p_0.$$

Coherence between the outgoing and the incoming waves can be maintained as long as the change of momentum, $p_0 - p$, is smaller than the inverse of the size R of the target. For $R = 1$ fm, one finds $M^2/s \leq 0.2$ which represents a kind of upper limit. High-energy data indeed provide clear evidence for diffractive production up to $M^2 \sim 0.05$ s.

At high energy it becomes very difficult to isolate specific exclusive channels where X is a known resonance. Most studies of diffraction dissociation in the exclusive channels were done at CMS energies less than 20 GeV and only a few in the energy range of the ISR (Amaldi *et al* 1976, Alberi and Goggi 1981).

At the high-energy colliders, experimental activity was limited to the study of inclusive diffraction where only the mass and the fragmentation properties of the system X are measured. In the process

$$\bar{p} + p \rightarrow \bar{p} + X \quad (48)$$

(or in the equivalent one $\bar{p} + p \rightarrow X + p$) the momentum vector k_f of the \bar{p} (or p) in the final state is measured in coincidence with the decay products of the system X which are emitted in the opposite hemisphere. It is usual to define the variable $x = k_f/k$, where k is the initial momentum in the CMS. The momentum transfer to the antiproton can then be written as

$$-t = m^2(1-x)^2/x + 2p_0^2x(1-\cos\theta)$$

where θ is the \bar{p} scattering angle and m is the proton mass. The mass M of the system X is given by $M^2 = (1-x)s$.

The coherence condition which sets a limit on the mass of the system X , also implies a special kinematical structure for the diffractive events with the existence of a large 'rapidity gap' between the 'leading' antiproton which is scattered in a quasi-elastic way and the decay products of X . We recall the definition of the rapidity y of a particle having energy E and longitudinal momentum p_1

$$y = \frac{1}{2} \log \frac{E + p_1}{E - p_1}.$$

Diffractive events have the typical rapidity configuration shown in figure 34. The scattered \bar{p} having lost in the collision only a small fraction of its momentum emerges with rapidity very close to the beam rapidity $y_0 = \log(\sqrt{s}/m)$. The system X has rapidity $y_X = \log(\sqrt{s}/M)$ and its decay products will have rapidities which cluster around y_X . It has been shown (Albrow *et al* 1976a, Bernard *et al* 1986a) that this cluster has elongated shape in phase space. Particles produced have limited transverse momentum ($\langle p_t \rangle \simeq 400$ MeV/c) and spread out in rapidity by the amount $\Delta y = \pm \log(\sqrt{s}/M)$. The average multiplicity of the diffractive cluster of invariant mass M was found to be the same as in hadronic collision with CMS energy equal to M (figure 35).

The identification of diffractive events at the high-energy colliders relies heavily on these distinctive kinematical features.

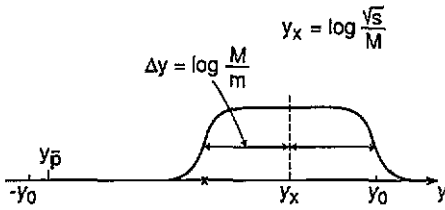
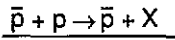


Figure 34. Rapidity structure of single diffraction-dissociation events.

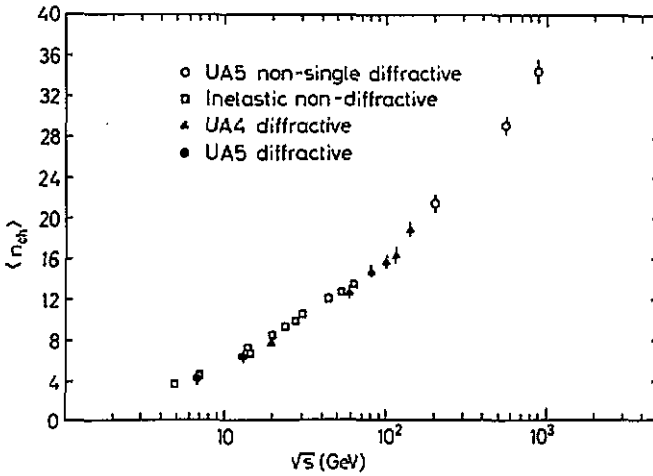


Figure 35. The average charge multiplicity of the diffractive cluster is compared with the overall charge multiplicity of non-diffractive events. Data from Ansonge *et al* (1986), Bernard *et al* (1986a) and Breakstone *et al* (1984b).

9.2. Differential distributions

Data on the inclusive reaction (48) are expressed in terms of the invariant differential cross section

$$E \frac{d^3\sigma}{d^3p} = \frac{s}{\pi} \frac{d^2\sigma}{dM^2 dt} = \frac{1}{\pi} \frac{d^2\sigma}{dx dt} \tag{49}$$

where $M^2 = (1 - x)s$. When plotted as a function of x , at fixed t , the cross section (49) exhibits the quasi-elastic peak at $x \sim 1$ which is typical of the diffractive process.

In the CHLM experiment at the ISR (Albrow *et al* 1976b), it was observed that the cross section (49), at fixed t , scales with the CMS energy with respect to the variable x , i.e. at fixed t and M^2/s , the invariant cross section does not change with energy. This property was found to remain valid up to the SPS collider energy as shown in figure 36 where the UA4 data at $\sqrt{s} = 546$ GeV (Bozzo *et al* 1984a) are presented together with earlier ISR results (Albrow *et al* 1976b). The scaling property only breaks down at very low masses because the minimum mass that can be excited, $M_{\min} \simeq m + m_{\pi}$, is independent of s .

Diffractive dissociation was recently observed at the Fermilab Tevatron by the CDF collaboration (Abe *et al* 1993). At these large energies, diffractive excitation of quite heavy

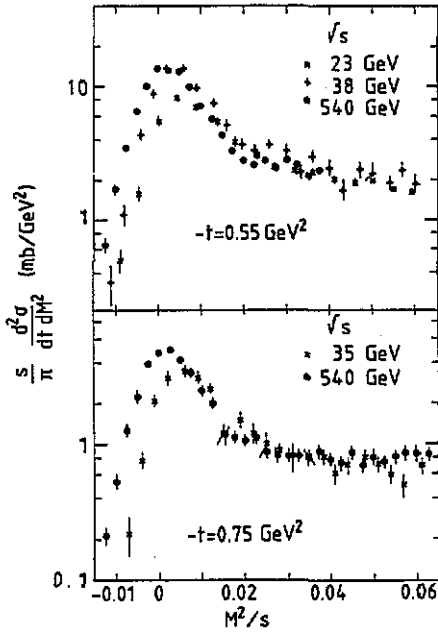


Figure 36. Scaling of the invariant differential cross section from $\sqrt{s} = 23$ GeV up to $\sqrt{s} = 540$ GeV for two values of the momentum transfer t . The quasi-elastic peak of diffractive events emerges at $M^2/s < 0.03$.

systems may take place. At $\sqrt{s} = 1.8$ TeV, in fact, the mass corresponding to $x = 0.98$ is as large as 250 GeV.

In the Regge model the dominant contribution to the cross section of diffraction dissociation is given by Pomeron exchange which can be written as

$$s \frac{d^2\sigma}{dM^2 dt} = H(t) \left(\frac{s}{s_0}\right)^{\alpha_P(0)-1} \left(\frac{s}{M^2}\right)^{2\alpha_P(t)-\alpha_P(0)} \quad (50)$$

where $\alpha_P(t)$ is the Pomeron trajectory.

For $\alpha_P(0) = 1$ the mass distribution $d\sigma/dM^2$ at low t would have the form $1/M^2$. This behaviour of the mass spectrum was found to hold, at least approximately up to the ISR energies (Goulianos 1983). Recently, however, Abe *et al* (1993) have reported that at the Tevatron energy the spectrum is slightly steeper. They fitted the measured distributions with (50) using for the Pomeron trajectory the expression

$$\alpha_P(t) = 1 + \epsilon + \alpha'_P t$$

which implies for the mass spectrum at $t \approx 0$ the form

$$\frac{d\sigma}{dM^2} \sim \left(\frac{1}{M^2}\right)^{1+\epsilon}$$

They assumed $\alpha'_P = 0.25$ GeV⁻² as suggested by the Regge analysis of the elastic scattering data (section 8.3). From the best fit it was found that $\epsilon = 0.125 \pm 0.015$, a value which compares reasonably well with the intercept of the Pomeron trajectory obtained directly from the rate of growth of the total cross sections (section 4).

A new approach to the study of the properties of the Pomeron was proposed by Ingelman and Schlein (1985). Such a study involves observation of jets in diffractive events at large momentum transfer and was performed by experiment UA8 at the SPS collider (Brandt *et al* 1992).

9.3. The integrated cross section σ_{SD}

The extraction of the integrated cross section of single diffraction dissociation σ_{SD} from the observed differential distribution $d^2\sigma/dxdt$ is affected by several uncertainties and is partly model dependent.

Results on σ_{SD} from the CHLM (Armitage *et al* 1982), the UA4 (Bernard *et al* 1987a) and the CDF experiment (Abe *et al* 1993) are presented in figure 37, already multiplied by a factor of two to account for the symmetric process. These data refer to the kinematical interval, $x > 0.95$, i.e. $M^2/s < 0.05$ where the peak of the diffractive events dominates over the continuum (figure 36).

These measurements were performed by detecting in a magnetic spectrometer the 'leading' particle recoiling against the system X in coincidence with the decay products of X , observed in a large acceptance vertex detector. The results from CHLM and CDF were obtained directly by integrating the observed mass spectra while the result from UA4 relied on an analysis of the 'rapidity gap'. This may be the reason for the discrepancy between the two results at $\sqrt{s} = 546$ GeV.

It is evident, however, that the cross section of diffraction dissociation grows with energy much less rapidly than the elastic and the total cross section. This is clearly demonstrated in figure 38 where the ratios σ_{el}/σ_{tot} and σ_{SD}/σ_{tot} are plotted as a function of energy.

The different behaviour of σ_{SD} with respect to σ_{el} can be understood within the general picture of Good and Walker (1960). In their discussion of the interaction of hadrons with nuclei they noted that a hadron, being a complex system, can be described as a linear combination of eigenstates having the same quantum numbers. If these eigenstates are absorbed differently in nuclear matter, the diffracted wave will have a composition different from the incoming wave. The consequence is the appearance of new physical states with the same quantum number as the proton, i.e. diffractive dissociation. If, however, all different hadronic components are equally affected by the interaction, no diffractive dissociation will occur. This would happen in the limiting case when there is full absorption.

The trend of the present data, as illustrated by the energy evolution of the shadow function $G_{in}(b)$ in figures 7 and 8, is indeed in this direction. It appears, therefore, that the rise of the ratio σ_{el}/σ_{tot} and the decrease of σ_{SD}/σ_{tot} are correlated, as discussed, for example, by Barshay *et al* (1992).

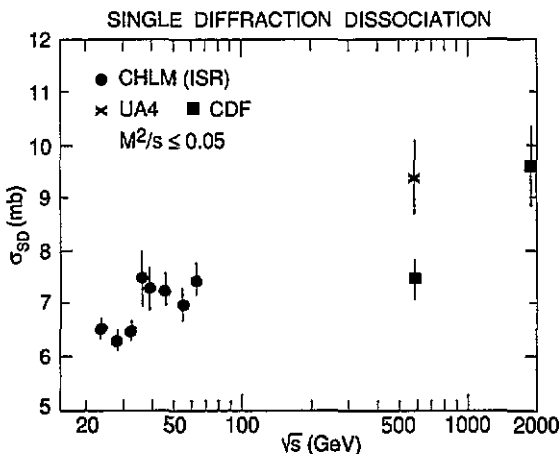


Figure 37. The cross section of single diffraction dissociation, defined by the kinematical condition $M^2/s \leq 0.05$, is shown as a function of energy.

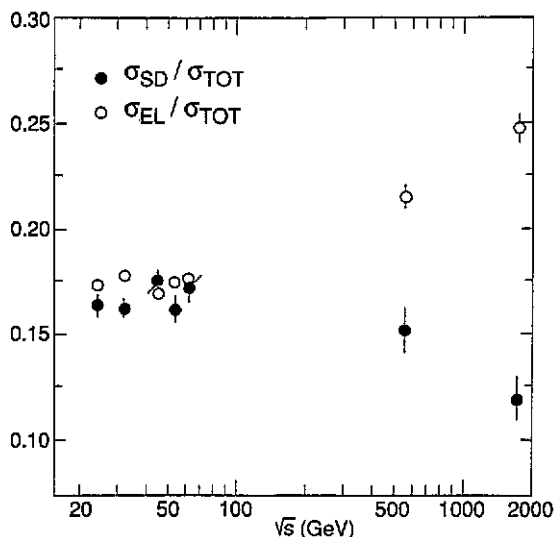


Figure 38. The ratio of the elastic to the total cross section σ_{el}/σ_{tot} , and the ratio of the single diffraction dissociation to the total cross section σ_{SD}/σ_{tot} , are shown as a function of energy.

10. Conclusions and outlook

We have at present a good phenomenological understanding of hadron–nucleon scattering up to the maximum energy explored by existing accelerators. The data are successfully described by two competing approaches.

- (1) The Regge model, a t -channel approach which evolved from the original simple formalism, adequate only at small momentum transfer, to the present rather sophisticated form with ‘eikonalization’ of the amplitude.
- (2) The diffraction models, a typical s -channel approach which relies on intuitive motivations.

These two approaches are to some extent complementary and both useful as a general framework for the understanding of the large amount of experimental results.

The ‘QCD-inspired’ models try to establish a connection between the old notions as ‘Pomeron trajectory’ and ‘hadron opacity’ and the new concepts based on the elementary interaction of quarks and gluons which represents the underlying structure.

Calculations performed within perturbative QCD seem to be of only limited relevance for the understanding of low-momentum-transfer processes. The first steps in the direction of non-perturbative calculations are still partly qualitative but appear to be rather promising.

On the experimental side it should be stressed that the measurements of the total cross section and of the real part at the high-energy colliders are technically difficult. Some efforts should still be spent to reduce systematic errors and improve the reliability of the results.

In perspective, new information will be gathered at the future hadron colliders.

- (1) The ‘relativistic heavy-ion collider’ (RHIC) at BNL will produce proton–proton collisions at $\sqrt{s} = 500$ GeV with high luminosity. The comparison of pp measurements from RHIC to the existing $\bar{p}p$ data from the SPS collider which are practically at the same energy will be quite interesting and instructive. In addition, RHIC allows measurements of elastic scattering to be performed in the large-momentum-transfer region, not accessible at the $\bar{p}p$ colliders because of their intrinsic limitation in luminosity.
- (2) The ‘large-hadron collider’ (LHC) at CERN will provide proton–proton collisions at $\sqrt{s} = 16$ TeV with very high luminosity. This new accelerator, probably operational

at the very beginning of the next century, will open a new energy domain and perhaps bring unexpected changes to our present ideas.

References

- Abe F *et al* (CDF collaboration, presented by Giromini P) 1993 *Proc. 5th Blois Workshop on Elastic and Diffractive Scattering* ed Fried, Kang and Tan (Singapore: World Scientific)
- Alberi G and Goggi G 1981 *Phys. Rep.* **74** 1
- Albrow M G *et al* 1976a *Nucl. Phys. B* **102** 275
- Albrow M G *et al* 1976b *Nucl. Phys. B* **108** 1
- Albrow M G 1993 *Proc. 5th Blois Workshop on Elastic and Diffractive Scattering* ed Fried, Kang and Tan (Singapore: World Scientific)
- Ajmer G J *et al* 1986 *Z. Phys. C* **32** 133
- Amaldi U *et al* 1973 *Phys. Lett.* **44B** 112
- Amaldi U *et al* 1977 *Phys. Lett.* **66B** 390
- Amaldi U *et al* 1978 *Nucl. Phys. B* **145** 367
- Amaldi U, Jacob M and Matthiae G 1976 *Ann. Rev. Nucl. Sci.* **26** 385
- Amaldi U and Schubert K R 1980 *Nucl. Phys. B* **166** 301
- Amendolia S R *et al* 1973 *Phys. Lett.* **44B** 119
- Amos N A *et al* 1985 *Nucl. Phys. B* **262** 689
- Amos N A *et al* 1990a *Phys. Lett.* **243B** 158
- Amos N A *et al* 1990b *Phys. Lett.* **247B** 127
- Amos N A *et al* 1992 *Phys. Rev. Lett.* **68** 2433
- Ansorge R E *et al* 1986 *Z. Phys. C* **33** 175
- Armitage J C M *et al* 1982 *Nucl. Phys. B* **194** 365
- Auberson G, Kinoshita T and Martin A 1971 *Phys. Rev. D* **3** 3185.
- Augier C *et al* 1993a *Phys. Lett.* **315B** 503
- Augier C *et al* 1993b *Phys. Lett.* **316B** 448
- Baltrusaitis R M *et al* 1984 *Phys. Rev. Lett.* **52** 1380
- Barbiellini G *et al* 1972 *Phys. Lett.* **39B** 663
- Barshay S 1972 *Phys. Lett.* **42B** 457
- Barshay S and Goldberg J 1987 *Phys. Lett.* **196B** 566
- Barshay S, Heiliger P and Rein D 1992 *Z. Phys. C* **56** 77
- Bernard D *et al* 1986a *Phys. Lett.* **166B** 459
- Bernard D *et al* 1986b *Phys. Lett.* **171B** 142
- Bernard D *et al* 1987a *Phys. Lett.* **186B** 227
- Bernard D *et al* 1987b *Phys. Lett.* **198B** 583
- Bethe H A 1958 *Ann. Phys.* **3** 190
- Block M M *et al* 1990 *Phys. Rev. D* **41** 978
- Bosser J *et al* 1985 *Nucl. Inst. Meth. A* **235** 689
- Bourrely C, Soffer J and Wu T T 1984 *Nucl. Phys. B* **247** 15
- Bourrely C, Soffer J and Wu T T 1988 *Z. Phys. C* **37** 369
- Bourrely C, Soffer J and Wu T T 1990 *Phys. Lett.* **252B** 287
- Bozzo M *et al* 1984a *Phys. Lett.* **136B** 217
- Bozzo M *et al* 1984b *Phys. Lett.* **147B** 385
- Bozzo M *et al* 1984c *Phys. Lett.* **147B** 392
- Bozzo M *et al* 1985 *Phys. Lett.* **155B** 197
- Brandt A *et al* 1992 *Phys. Lett.* **297B** 417
- Breakstone A *et al* 1984a *Nucl. Phys. B* **248** 253
- Breakstone A *et al* 1984b *Phys. Rev. D* **30** 528
- Breakstone A *et al* 1985 *Phys. Rev. Lett.* **54** 2180
- Bronzan J B, Kane G L and Sukhatme U P 1974 *Phys. Lett.* **49B** 272
- Burq J P *et al* 1983 *Nucl. Phys. B* **217** 285
- Buttimore N H, Gotsman E and Leader E 1978 *Phys. Rev. D* **18** 694
- Cahn R 1982 *Z. Phys. C* **15** 253
- Carboni G *et al* 1985 *Nucl. Phys. B* **254** 697
- Castaldi R and Sanguinetti G 1985 *Ann. Rev. Nucl. Part. Sci.* **35** 351

- Cheng H and Wu T T 1969 *Phys. Rev. Lett.* **22** 666; 1969 *Phys. Rev.* **186** 1611
 Cheng H and Wu T T 1970 *Phys. Rev. Lett.* **24** 1456; 1970 *Phys. Rev. D* **1** 2775
 Cheng H and Wu T T 1987 *Expanding Protons—Scattering at High Energies* (Cambridge, MA: MIT Press)
 Chew G F 1961 *S-matrix Theory of Strong Interactions* (New York: Benjamin)
 Chou T T and Yang C N 1968 *Phys. Rev. Lett.* **20** 1213
 Chou T T and Yang C N 1979 *Phys. Rev. D* **19** 3268
 Chou T T, Wu T T and Yang C N 1982 *Phys. Rev. D* **26** 328
 Collins P D B 1977 *An Introduction to Regge Theory* (Cambridge: Cambridge University Press)
 Cornille H and Martin A 1972 *Nucl. Phys. B* **48** 104
 Covolan R M J *et al* 1992 *Nucl. Phys. B (Proc. Suppl.)* **25** 86
 Covolan R M J *et al* 1993 *Z. Phys. C* **58** 109
 Dias de Deus J 1973 *Nucl. Phys. B* **59** 231
 Dias de Deus J and Kroll P 1978 *Acta Phys. Pol. B* **9** 159
 Dias de Deus J and Kwieciński J 1987 *Phys. Lett.* **196B** 537
 Donnachie A and Landshoff P V 1979 *Z. Phys. C* **2** 55
 Donnachie A and Landshoff P V 1983 *Nucl. Phys.* **231B** 189
 Donnachie A and Landshoff P V 1984 *Nucl. Phys.* **244B** 322
 Donnachie A and Landshoff P V 1986 *Nucl. Phys.* **267B** 690
 Donnachie A and Landshoff P V 1992 *Phys. Lett.* **296B** 227
 Dosch H G and Ferreira E 1993 *Phys. Lett.* **318B** 197
 Dosch H G, Ferreira E and Krämer 1992 *Phys. Lett.* **289B** 153
 Durand L and Lipes R 1968 *Phys. Rev. Lett.* **20** 637
 Durand L and Pi H 1989 *Phys. Rev. D* **40** 1436
 Ellis R K and Scott W G 1989 *Proton–Antiproton Collider Physics* ed Altarelli and Di Lella (Singapore: World Scientific) p 131
 Faissler W *et al* 1981 *Phys. Rev. D* **23** 33
 Fischer J 1981 *Phys. Rep.* **76** 157
 Froissart M 1961 *Phys. Rev.* **123** 1053
 Gauron P, Leader E and Nicolescu B 1988 *Nucl. Phys.* **B299** 640
 Gauron P, Lipatov L and Nicolescu B 1993 *Phys. Lett.* **B304** 334
 Glauber R J 1959 *Boulder Lectures on Theoretical Physics* (New York) vol 1 p 315
 Glauber R J 1969 *Proc. Third Int. Conf. on High-energy Physics and Nuclear Structure* (New York) p 207
 Glauber R J and Velasco J 1984 *Phys. Lett.* **147B** 380
 Glauber R J and Velasco J 1988 *Proc. Second Int. Conf. on Elastic and Diffractive Scattering* (New York) p 219
 Good M L and Walker W D 1960 *Phys. Rev.* **120** 1857
 Goulianos K 1983 *Phys. Rep.* **101** 169
 Grunberg G and Truong T N 1973 *Phys. Rev. Lett.* **31** 63
 Haguenauser M and Matthiae G 1984 *Proc. ECFA-CERN Workshop on Large Hadron Collider in the LEP Tunnel* vol 1 p 303
 Halzen F 1993 *Proc. 5th Blois Workshop on Elastic and Diffractive Scattering* ed Fried, Kang and Tan (Singapore: World Scientific)
 Henzi R and Valin P 1983 *Phys. Lett.* **132** 443
 Henzi R and Valin P 1985 *Phys. Lett.* **160** 167
 Honda M *et al* 1993 *Phys. Rev. Lett.* **70** 525
 Ingelman G and Schlein P 1985 *Phys. Lett.* **152B** 256
 Islam M M 1992 *Nucl. Phys. B (Proc. Suppl.)* **B 25** 104
 Jenkovszky L, Paccanoni F and Predazzi E 1992 *Nucl. Phys. B (Proc. Suppl.)* **B 25** 80
 Kang K and Nicolescu B 1975 *Phys. Rev. D* **11** 2461
 Khuri N N and Kinoshita T 1965 *Phys. Rev. B* **137** 720
 Koba Z, Nielsen H B and Olesen P 1972 *Nucl. Phys. B* **40** 317
 Kroll P 1983 *Proc. XVIII Rencontre de Moriond* p 81
 Kundrat V and Lokajicek M 1993 *CERN Internal report* CERN-TH 6952/93
 Landshoff P V 1991 *Proc. 1991 HEP Conference (Geneva)* vol 2 p 363
 Levin E M and Ryskin M G 1990 *Phys. Rep.* **189** 267
 L'Heureux P, Margolis B and Valin P 1985 *Phys. Rev. D* **32** 1681
 Lipatov L N 1986 *JETP* **63** 904
 Lipatov L N 1989 *Perturbative Quantum Chromodynamics* ed Mueller (Singapore: World Scientific) p 411
 Lukaszuk L and Martin A 1967 *Nuovo Cimento A* **52** 122

- Lukaszuk L and Nicolescu B 1973 *Nuovo Cimento Lett.* A 52 122
MacDowell S W and Martin A 1964 *Phys. Rev.* B 135 960
Margolis B *et al* 1988 *Phys. Lett.* 213B 221
Martin A 1966 *Nuovo Cimento* 42 930; 44 1219
Martin A 1993 *CERN Internal report* CERN-TH 6894/93
Martin A and Matthiae G 1989 *Proton-Antiproton Collider Physics* ed Altarelli and Di Lella (Singapore: World Scientific) p 45
Menon M J 1992 *Nucl. Phys. B (Proc. Suppl.)* B 25 94
Nachtmann O 1991 *Ann. Phys.* 209 436
Nagy E *et al* 1979 *Nucl. Phys.* B 150 221
Pomeranchuk I Ya 1958 *JETP* 7 499
Pumplin J 1992 *Phys. Lett.* 289B 449
Roy S M 1972 *Phys. Rep.* C 5 125
Singh V and Roy S M 1970 *Phys. Rev.* 1 2638
Söding P 1964 *Phys. Lett.* 8 285
Van der Meer S 1968 *CERN Internal report* ISR-PO/68-31
Van Hove L 1964 *Rev. Mod. Phys.* 36 655
Ward D R 1989 *Proton-Antiproton Collider Physics* ed Altarelli and Di Lella (Singapore: World Scientific) p 85
West G B and Yennie D R 1968 *Phys. Rev.* 172 1413